MASS-GAPS IN LATTICE FIELD THEORIES

Thesis by

Rajan Gupta

In Partial Fulfillment of the Requirements

for the Degree of

Doctor of Philosophy

California Institute of Technology

Pasadena, California.

1982

(Submitted May 3 ,1982)

ACKNOWLEDGEMENTS

I sincerely thank my advisor Geoffery Fox for his encouragement and support over these last few years. No less a word of thanks goes to Rick Field for having initiated me into the family and having watched over my feeble attempts at flight.

I thank my collaborators, S. Otto, Lee Chang and O. Martin for cheerfully putting up with my eccentricities and for their help. I owe my learning and skills to numerous members of the family and to them I pledge to work honestly.

It is a pleasure to thank R. P. Feynman, David Politzer and Larry Yaffe for many enlightening discussions that helped me understand the subject.

The midnight toil would have been barren had it not been for the warmth of many around me. Names come to my mind in a frantic rush: Louise Sartain, Mark Bowick, Helen Tuck, Sarabmeet Kanwal, P. K. Aravind, Hideaki Aoyama, Mike Shatz, Mohit Randeria, Apoorva Patel, J. Kim, Rick Brenner, Sanjay Tiwari, R. Jha, Lavleen Singal, J. Bajaj, John Valainis, David Iskandar, Norman Wilson, ... and John Osborne for trying to convince me that I lead a charmed existence. As for Gayle, a few words of acknowledgement could not even begin to express my appreciation.

And finally to my parents, who provided all the love, support and encouragement that is humanly possible, I dedicate this thesis as a small token of gratitude.

ABSTRACT

In this thesis we discuss two methods for calculating the mass-spectrum in field theories using Monte Carlo Methods. A Hamiltonian variational method is developed and checked on the O(3) non-linear sigma model in 1+1 dimensions. The mass-gap is also found from the 2-point correlation function and some improvements to this method are suggested. Both methods give reliable results for the lattice theory. The connection between the lattice O(3) spin-model and the continuum theory is explored in detail.

Table of Contents

INTRODUCTION

A question that we would like to see answered is , what are the fundamental constituents of matter and what is the underlying dynamical theory that describes their interactions? For the last ten years there has been only one candidate for the theory of strong interactions: Quantum Chromodynamics (QCD). In this theory the hadrons are made up of spin 1/2 particles called quarks which interact by the exchange of massless vector bosons called gluons. The charge of the quark comes in three colors, and the theory has an exact local gauge symmetry such that the interactions do not distinguish between the colors. This theory is elegant, compatible with all experimental data and yet elusive. The reason being that no one has been able to calculate precise numbers from it. The eventual goal is to be able to calculate both the static (hadron masses, magnetic moments) and dynamical (scattering) properties of strong interactions in terms of the basic parameters in the Lagrangian. These are the coupling constant g and the quark masses which, at this level, we take to be inputs. This thesis is an attempt to understand some of its features and develop numerical techniques to solve it.

QCD is a non-linear field theory for which a closed form solution is not known, so one has to resort to approximations. If one assumes that there is some region in which the QCD coupling constant is small then a perturbation expansion can be made. Such a perturbative calculation showed that $g=0$ is an ultra-violet stable fixed point of the theory[1]. In other words the theory can be described in terms of an effective coupling constant that goes to zero in the limit of large momenta. This property, called asymptotic freedom, allows one to use perturbation theory above some mass scale where the coupling constant is small. Present experiments fix this scale at a few Gev. Two problems arise in

using perturbative QCD to describe strong interaction phenomenon at large momentum transfers. The first is computational: The complexity of successive terms in the expansion grows exponentially. The second is that QCD describes the interaction of quarks and gluons while in experiments one observes color singlet composite states, the hadrons. It is therefore expected that before we can describe the interaction of hadrons, the problem of how quarks and gluons turn into hadrons needs to be solved. Unfortunately, this problem is not within the scope of Perturbative QCD so one has to model this part of the interaction. One successful scheme is to break up a given process with hadrons as asymptotic states into two parts. The non-perturbative part, in which the conversions of quarks and gluons into hadrons is described by phenomenological functions that are fixed by experiments, and the short distance behavior that can be calculated using perturbation theory. This separation has been carried out self-consistently for a number of inelastic processes. Unfortunately, a large amount of accurate experimental data is required to fix the phenomenological functions introduced. As a result detailed quantitative tests of the theory are lacking. We calculated the Pion Form Factor[2] to show that the methods used to study inelastic processes can also be used for elastic processes. The experimental data is poor, therefore a comparison of it with the calculation is not possible at present.

The QCD coupling constant is a function of the momentum transfer and is large at the hadron mass-scale. Thus low-energy phenomenon are not accessible to perturbation theory. Wilson[3] provided an alternative by defining the theory on a lattice and developing a strong coupling expansion. This did not totally solve the problem because to get rid of the lattice artifacts one is required to study the theory near zero bare coupling. Therefore very high powers of the expansion are required. Later Wilson[4] and Creutz[5] showed

that the lattice theory is ideally suited to Monte Carlo simulations and that a number of low-energy non-perturbative features can be calculated numerically. In chapter 2, a brief review of lattice QCD and the status quo of Monte Carlo results is presented.

The hadronic mass-spectrum is one of the quantities that can be calculated using Monte Carlo techniques. In chapter 3 we investigate two methods for the calculation of mass-gaps in field theories. The 2-point correlation method is well known from Solid State Physics and some improvements on it are discussed in section (3.3). An additional Hamiltonian variational method is developed and tested on the non-linear Sigma model in 1+1 dimensions. This model has a number of features in common with QCD. It is asymptotically free and confining, and therefore an ideal model in which to test these Monte Carlo methods with a modest outlay of computer time. An essential ingredient of any Monte Carlo calculation is to have a control over the statistical errors. Model field theories in 1+1 dimensions are very useful in gaining this experience. We have therefore spent considerable time investigating sources of errors, statistics and methods in 1+1 dimensions rather than work in 4-dimensions where such details would have required prohibitive amounts of computer time. A significant portion of this chapter has been published[6].

A crucial feature of the Monte Carlo calculations is that in order to study the behavior of the theory in the continuum limit, one is forced to use the weak coupling renormalization group to extrapolate the results from some finite lattice spacing. The lattice provides a ultra-violet cutoff that is different from the cutoffs introduced to regulate the continuum theory. The definition of the coupling constant depends on the regularization scheme, consequently the relation between the lattice coupling and the continuum coupling has to be found. This calculation for the O(3) model is shown in chapter 4.

REFERENCES

[1] H. D. Politzer, Phys. Rev. Lett. 30 (1973) 1346.

D. Gross and F. Wilczek, Phys. Rev. Lett. 30 (1973) 1343.

[2] R. D. Field, R. Gupta, S. Otto and Lee Chang, Nucl. Phys. B186 (1981) 429.

R. Gupta, *Proceedings of the AIP Conference On Perturbative Quantum Chromodynamics, Tallahassee, Florida.* 1981, AIP, New York, 1981.

[3] K. Wilson, Phys. Rev. D10 (1974) 2445.

[4] K. Wilson, Cargese lectures (1979).

[5] M. Creutz, Phys. Rev. Lett. 43 (1979) 553.

[6] G. Fox, R. Gupta, O. Martin and S. Otto, Nucl. Phys. B205[FS5] (1982) 188.

REVIEW OF LATTICE GAUGE THEORIES

2.1: Introduction

In this chapter a brief review of Lattice Gauge theories is presented along with the results obtained for them using Monte Carlo methods. Since the simulations of SU(3) in four dimensions are extremely slow, simpler models in fewer dimensions are indispensable for gaining valuable experience and intuition. Therefore the goal is twofold: To learn how best to write a field theory on a lattice and to develop Monte Carlo methods to study it. The particular theory we are interested in at present is QCD, therefore the formalism will be set up for it. Existing results and methods are reviewed to find their strengths and weaknesses.

The number of variables in any field theory are infinite, one per internal degree of freedom at each space-time time point. The first approximation is to make the number of variables finite by defining the theory on a hypercubical lattice of finite extent. Periodic boundary conditions are imposed to remove surface effects. The finite lattice spacing $\delta x = a$ also provides a high momentum cutoff so that there are no ultra-violet divergences. The lattice observables are therefore functions of the bare parameters in the Lagrangian and this cutoff. The aim is to find the renormalized values in the limit $a \to 0$.

In the real time formulation of quantum mechanics, there is an amplitude of unit magnitude associated with each path by which a system can evolve from a given initial state to some final state[1]. This phase is e^{iS}, where S is the action measured in units of the Planck's constant. In constructing the probability for the transition, these phases interfere and the maximum contribution comes from paths with the minimum action. This is easier to visualize if we

define the Quantum theory via the Euclidean Feynman Path Integral. The eigenvalues and the eigenvectors of the theory are unchanged by this transformation $it \rightarrow \tau$, but the complex phase turns into an exponentially damping factor e^{-S} where

$$S = \int_0^\beta H d\tau. \tag{2.1.1}$$

The field-theory now becomes a Statistical Mechanical problem, with a probability for each path. One can therefore use Monte Carlo methods to evaluate the Path integral. In Eq.(2.1.1), β is the inverse of the real physical temperature. Due to the exponential damping, in the limit $\beta \rightarrow \infty$ only the ground state contributes and the system is said to be at zero temperature. On the lattice this is approximated by taking the lattice size in the time direction, N_τ, much larger than the correlation length ξ. This introduces corrections that are of the order of $e^{\frac{-N_\tau}{\xi}}$. To study the behavior of the system as a function of the temperature, all that needs to be done is to vary N_τ and use the connection

$$Temp = \frac{1}{N_\tau a}. \tag{2.1.2}$$

In the following review we shall restrict ourselves to the zero-temperature limit unless otherwise stated.

The generating functional for lattice QCD can be written in the form

$$\Xi = \int DU\, D\bar{\Psi}\, D\Psi\, e^{-\beta S_G + \bar{\Psi}_i M(U)_{ij} \Psi_j} \tag{2.1.3}$$

where S_G is the action for the gauge fields, i and j correspond to lattice sites and all internal indices have been suppressed. For the theories of interest the fermionic action can be written in the bilinear form, $\Psi_i M_{ij} \Psi_j$, where M_{ij} includes the kinetic, mass and the gauge-fermion coupling terms. At the outset

we would like to point out that different lattice S_G and M_{ij} lead to the same continuum theory. This is because one can add terms to the lattice action that either vanish as the spacing a goes to zero or have the same local structure. More will be said about this non-uniqueness of the lattice action in the course of the discussion.

In Wilson's formulation of the theory[2], the gauge degrees of freedom, U_{ij}, are defined on directed links connecting the sites $i \rightarrow j$ and are elements of the gauge group. The reversed link is by definition the inverse element

$$U_{i,j} = (U_{j,i})^{-1}. \tag{2.1.4}$$

In the continuum theory, the motion of a quark between two points in the presence of the gauge fields picks up a phase that is the exponential of the path-ordered line integral of the gauge fields between the two points, i.e.,

$$\Psi_f = \exp\left[ig \int_i^f dx^\mu \frac{\vec{\lambda}}{2}\cdot\vec{A}_\mu(n) \right] \Psi_i. \tag{2.1.5}$$

The elements $U_{i,j}$ are just these phases, so on the lattice the connection between them and the colored gauge fields A^a_μ is given by

$$U_\mu(n) = \exp\left[iag \frac{\vec{\lambda}}{2}\cdot\vec{A}_\mu(n) \right] \tag{2.1.6}$$

where $U_\mu(n)$ is the link in the μ direction at site n and λ are the group matrices that are specified by the fermion representation. Consequently the fermi- degrees of freedom Ψ_i are defined on the lattice sites. Under a local gauge transformation Ω, U_{ij} and Ψ_i transform as

$$\Psi_i \rightarrow \Omega_i \psi_i$$

$$U_{i,j} \rightarrow \Omega_i U_{i,j} \Omega_j^{-1}. \tag{2.1.7}$$

There are two kinds of operators that are invariant under these local gauge transformations:

1) Closed loops of gauge fields. The simplest such is an elementary plaquette ▫, the product of four U's around a square.

$$S_{\square} = U_{\mu}(n)\,U_{\nu}(n+\mu)\,U_{-\mu}(n+\mu+\nu)\,U_{-\nu}(n+\nu) \tag{2.1.8}$$

2) Wilson strings

$$\Psi_i\, U_{i,j} \ldots\ldots\ldots U_{k,l}\,\Psi_l . \tag{2.1.9}$$

The action is to be constructed out of these gauge invariant quantities and should have the known continuum limit. The simple plaquette

$$S_{\square} = U_{\mu}(n)\,U_{\nu}(n+\mu)\,U_{-\mu}(n+\mu+\nu)\,U_{-\nu}(n+\nu)$$

$$\xrightarrow[a\to 0]{} \exp\left[\, ia^2 g\ \frac{\vec{\lambda}}{2}\cdot\vec{F}_{\mu\nu}\,\right] \tag{2.1.10}$$

where

$$F^{a}_{\mu\nu} = \partial_{\mu}A^{a}_{\nu} - \partial_{\nu}A^{a}_{\mu} + g\, f^{abc}\, A^{b}_{\mu}\, A^{c}_{\nu}. \tag{2.1.11}$$

Wilson therefore defined

$$S_G = \sum_{\square}\left(1 - \frac{1}{N}\,Tr\; S_{\square}\right) + c.c. \tag{2.1.12a}$$

$$\xrightarrow[a\to 0]{} \frac{g^2}{2N}\,\frac{1}{4}\int d^4x\ \ \vec{F}_{\mu\nu}\,\vec{F}^{\mu\nu} \tag{2.1.12b}$$

as the action for SU(N) gauge fields, with the identification

$$\beta = \frac{2N}{g^2}. \tag{2.1.13}$$

It is common practice to call this coupling constant β the inverse temperature also. This is a misnomer, and to avoid confusion we shall not do so.

The fermion action can be written as

$$S_F = -\sum_i \bar{\Psi}_i \Psi_i + K \sum_{i,\mu} \left[\bar{\Psi}_i (r - \gamma_\mu) U_\mu(i) \Psi_{i+\mu} + \bar{\Psi}_{i+\mu} (r + \gamma_\mu) U_\mu^\dagger(i) \Psi_i \right]$$

$$\equiv \sum_{ij} \bar{\Psi}_i M_{ij} \Psi_j. \qquad (2.1.14)$$

The two cases of interest are:

1) r=0: This corresponds to replacing the derivative in the continuum action by a finite central difference. A simple rescaling of the fields $\sqrt{K}\ \Psi \to \Psi$ allows K to be interpreted as the reciprocal of the bare quark mass,i.e. $K=\frac{1}{2ma}$. Therefore the chiral behavior of the theory, for any value of g, can be studied in the limit $K \to \infty$ while keeping $\sqrt{K}\Psi$ constant. The drawback of this action is that in the continuum limit, the number of fermion modes proliferate. The dispersion relation shows that E -> m_0 at k=$\frac{\pi}{a}$ in addition to k=0. Therefore in d-dimensions one gets 2^d flavors instead of one. This problem can partly be overcome by placing only one spin degree of freedom at each lattice site instead of the full spinor. However the process of splitting the degrees of freedom to remove the degeneracy is clumsy and reduces the chiral symmetry to a discrete one[3]. In situations where the number of flavors are inconsequential, i.e. the chiral behavior of the theory, this is the preferred form of the action.

2) r=1: A non-zero r raises the energy of the modes at the boundary of the Brillouin cell and in the continuum limit, only the mode at k=0 survives. The relation between the bare quark mass, m, and K is found from the pole in the quark propagator, and for the free theory $\beta = \infty$ (all $U = 1$), is

$$K = \frac{1}{2ma + 8r}. \qquad (2.1.15)$$

Thus the chiral limit is at $K=\frac{1}{8r}$. For the interacting theory, Eq. (2.1.15) does not hold and the value of $K(g)$ at which the quark mass vanishes has to be defined in terms of a diverging correlation length. If one assumes that the mass of the pion is to first order linear in the quark mass, then the pole in the pion propagator can be used. On the other hand, to get the the observed mass-spectrum, $K(g)$ is fixed by requiring that the pion have a mass of 140 Mev. This form of the action is better suited for estimating the hadron masses.

In the generating functional for the Quantum theory, Eq.(2.1.3)

$$\Xi = \int DU\, D\bar{\Psi}\, D\Psi\, e^{-\beta S_G + S_F} \tag{2.1.16}$$

the fermi-fields are Grassmann variables and cannot be represented as such on the lattice. There are two solutions that allow a probability interpretation for them

1) The fermions are represented by their world lines and one calculates the elements of the transfer Matrix. These elements are taken to be the probability for moving a fermion at a given time step. Fermi-statistics, not allowing the lines to cross, is enforced by hand at each step. Hirsch et.al.[4] break up the Hamiltonian in such a way that the algorithm stays local. The path integral is the sum of all possible configurations of the world lines. This method has not been generalized to dimensions higher than two. Therefore we do not discuss it any further.

2) The approach that has been more successful is to note that the action S_F in Eq.(2.1.14) is bilinear in the fermi-fields, so they can be integrated out. The generating functional in the presence of sources η is

$$\Xi[\bar{\eta},\eta] = \int DU\, D\bar{\Psi}\, D\Psi\, e^{-\beta S_G + S_F + \sum_i (\bar{\Psi}_i \eta_i + \bar{\eta}_i \Psi_i)} \tag{2.1.17a}$$

which on integrating over the fermions becomes

$$= \int [DU]\, e^{-S_{eff}[U] + \sum_{ij} \bar{\eta}_i [M^{-1}(U)]_{ij} \eta_j} \tag{2.1.17b}$$

where M is the matrix defined in Eq.(2.1.14). The weight for a given gauge configuration is now given by an effective action S_{eff}

$$S_{eff} = \beta S_G + Tr \ln M[U]. \tag{2.1.18}$$

For a consistent probability interpretation $\det[M]$ should be positive. The expectation value of pure gauge operators is given by

$$\langle F[U] \rangle = \frac{1}{\Xi} \int DU\, F[U]\, e^{-S_{eff}} \tag{2.1.19}$$

while fermion correlation functions are found by differentiating with respect to the sources η

$$\langle \bar{\Psi}_i \Psi_j \rangle = \frac{\delta^2}{\delta \eta_i \delta \bar{\eta}_j} \ln \Xi [\bar{\eta}, \eta] \; |_{\bar{\eta}=\eta=0}$$

$$= \frac{1}{\Xi} \int DU\, M^{-1}_{ji}(U)\; e^{-S_{eff}}. \tag{2.1.20}$$

Thus all pure gauge observables and fermion correlation functions in the presence of dynamic fermions are averages over gauge configurations generated with a Boltzmann factor S_{eff}. However, both $\det M$ and M^{-1} are non-local and M is a very large matrix, its order grows as the volume of the system. The central technical problem left to solve in this approach is to find fast computer algorithms to evaluate these quantities. In the next section we discuss some of the known methods and their limitations. The results for the pure gauge theory are given in section (2.3) while in section(2.4) fermions are included.

2.2: NUMERICAL TECHNIQUES.

In this section we review some approximate methods for dealing with the determinant and inverse of extremely large sparse matrices M encountered in the Monte Carlo simulation of QCD. A brief description of how the Path Integral is evaluated stochastically by Monte Carlo method is given in section (4.4) and we refer the reader to it. The methods have loosely been grouped into the following three classes:

i) Introducing auxiliary Boson Fields[5].

ii) The hopping parameter or loop expansion[6].

iii) Stochastic method for inverting matrices[7].

The auxiliary boson fields are introduced to cancel the determinant M gotten from integrating out the fermions. The identity

$$\det M(U) \;=\; const \int D\Phi \exp\left[\, -\Phi_i \, M_{ij}^{-2}\,(U)\, \Phi_j \,\right] \tag{2.2.1}$$

where Φ is a real scalar field replaces the determinant by an extra Path integral in Eq.(2.1.17). The effective action for the update of gauge fields now becomes

$$S[U,\Phi] \;=\; \beta S_G \;+\; \sum_{i,j} \left[\, \Phi_i \, M_{ij}^{-2}\,(U)\, \Phi_j \,\right] \tag{2.2.2}$$

while the Φ are updated with the action

$$\sum_{i,j} \Phi_i \, M_{ij}^{-2}\,(U)\, \Phi_j \;. \tag{2.2.3}$$

The factor due to the boson field is still non-local, but it can be calculated by Gauss-Seidel iterations. Define $x_i(U) = M_{ij}^{-1}\,\Phi_j$ such that (repeated indices are summed over)

$$\Phi_i \, M_{ij}^{-2}\,(U)\, \Phi_j \;=\; x_i^{+}(U)\, x_i(U). \tag{2.2.4}$$

where, if the Matrix M is not hermitian then we require that M and M^+ should have the same spectrum. This is true for QCD. The solution of the linear system of equations

$$M_{ij}(U)\,\Phi_j \;=\; x_i \tag{2.2.5}$$

by repeated iterations is efficient because the matrix M is sparse. A judicious choice for the starting x_i at a given update is to use the previous x. The convergence of the iterates becomes slow near the continuum limit as the spectrum of M develops a zero eigenvalue(massless fermion). One therefore has to extrapolate to the massless limit[5]. The time required for each iteration grows as the volume of the lattice and one complete Gauss-Seidel sequence has to be carried out per link update. This makes the method impractical, at present, for 4-dimensional field theories.

To calculate the fermion correlation functions, we need M^{-1}. The propagator being translationally invariant, we need to calculate a few columns (for different spin projections) only of the inverse matrix. These are gotten by solving iteratively the system of equations

$$M_{ij}\;P_{jk} \;=\; \delta_{i,k} \tag{2.2.6}$$

for fixed k. P_{ik} is then the propagator between points i and k. Each such iteration also grows as the volume of the lattice, however in this case the calculation is done every few sweeps and not at each update. The limitation that remains is the lack of convergence near the continuum limit.

The hopping parameter expansion is a power series expansion in the dimensionless coupling constant K. This method is best suited to the Wilson action with $r=1$ in Eq.(2.1.14). If the fermion matrix is written as

$$M \;\equiv\; 1 - K\,O \tag{2.2.7}$$

where (suppressing spin and color indices)

$$O_{ij} = \sum_{\mu} \left[(1 - \gamma_\mu)\, U_\mu(i)\, \delta(i-j+\mu) + (1 + \gamma_\mu)\, U_\mu^{+}(i)\, \delta(i-j-\mu) \right] \quad (2.2.8)$$

then, we can write

$$Tr \ln (1 - KO) = Tr \sum_{n=1}^{\infty} \frac{K^n O^n}{n} \quad (2.2.9)$$

and

$$M^{-1} = \frac{1}{1 - KO} = \sum_{n=0}^{\infty} K^n O^n. \quad (2.2.10)$$

From the definition of the matrix O, the element ij of O^n is the sum of path-ordered product of the spin and color matrices along all possible strings of length n between the two points. The operation of trace in Eq.(2.2.9) implies that only closed loops survive. Thus in the update of a given link we have to consider all possible closed loops which include that link. The loops of a given length can be divided into distinct topological types. The product of the spin matrices for a given type is constant and can be calculated beforehand and stored. The numerical calculation of the path-ordered product of the color matrices along the loop is very slow. This is because the number of loops of a given length,n, grows exponentially. The order n at which the series should be truncated is controlled by the correlation length and this for confining theories also grows exponentially as the continuum limit is approached. Therefore this method is useful in a limited range of the coupling constant space.

An alternative is to combine the factor of the fermionic determinant with the propagator in the expectation value. The update can now be performed with just the pure gauge action. The propagator between any two points is given by the sum of all possible strings connecting them according to Eq.(2.2.10). To

include the effects of virtual quark loops in the calculation each string must be considered in the presence of all possible closed loops. This again makes the computation slow and limits one to regions of large g and away from the chiral limit. A random and/or weighted sampling of loops may make it reasonable. This remains to be seen.

In the update of a link $U \to \tilde{U}$, we only require the difference in the fermion action due to the change. If $\delta M = U - \tilde{U}$, then

$$\ln \det M[\tilde{U}] - \ln \det M[U] = \ln \det (1 + M^{-1}\, \delta M)$$

and to first order in δM

$$\longrightarrow Tr\ M^{-1}\, \delta M. \tag{2.2.11}$$

The Neumann series for M^{-1} is

$$(M^{-1})_{ij} = (\frac{1}{1-KO})_{ij} = \delta_{ij} + KO_{ij} + K^2 O_{il}\, O_{lj} + \ldots . \tag{2.2.12}$$

This is the same as the hopping parameter expansion, Eq.(2.2.10), except that Kuti[7] has suggested that it is more efficient to evaluate it stochastically. The method is as follows: Write each matrix element as

$$K\, O_{ij} = P_{ij} * R_{ij} \tag{2.2.13}$$

with the probabilities P_{ij} such that for all rows i

$$P_{ij} > 0 \qquad \text{for } all\ j$$

$$\sum_j P_{ij} = 1. \tag{2.2.14}$$

We are here considering the modified version[7] where the probability to stop the walk described below is zero. To find a given row i of the inverse matrix,

start a random walk at element ij selected with a probability P_{ij}. The next step in the random walk is an element jl on row j selected with probability P_{jl} and so on. At each step in the walk a score Θ_{ik} is kept (i is the starting row index and k is the column index at the end of that step), which is defined to be the product of the residues R_{ij} along the the walk,

$$\Theta_{ik} = R_{i,}R_{,,}R_{,,} \ldots\ldots R_{,j}. \tag{2.2.15}$$

This is nothing other than the path-ordered product along a string connecting the two points. Thus the expectation value of this variable Θ_{ij} is M_{ij}^{-1}. The first term δ_{ij} in Eq.(2.2.12) corresponds to walks stopping immediately, and is put in by hand. The exact number of walks required, and the length of each walk for a given accuracy depends on the size of the lattice only through the coupling constants (correlation length). In this sense the calculation time is independent of the lattice dimensions. The sparse nature of M yields only a few non-zero P_{ij} per row and the time required for each step is short. However the fluctuations in the value of a given matrix element fall only as $\frac{1}{\sqrt{N}}$ where N is the total number of scores kept. When the system starts to freeze, the walks wander far and the scores are distributed over an increasingly large number of elements. Thus for a given accuracy the walk length and the number of walks has to increase as some power of the correlation length. It is my intention to check this method for QCD in the near future.

The list of methods is by no means exhausted. Minor variations and combining different methods all lead to small improvements while what is needed is a few orders of magnitude. Thus, while the problem is well defined, Monte Carlo simulations with dynamic fermions is still in its infancy. The computer industry is booming and these numerical methods can anticipate a pampered upbringing. So, I for one will not hesitate to bet on them.

2.3: RESULTS FOR THE PURE GAUGE THEORY

The aim of the Monte Carlo calculation is to check whether the SU(3) color gauge theory is asymptotically free, confines color and has dynamical mass generation, i.e. massive glue-ball states. Asymptotic freedom implies that the theory has an ultra-violet fixed point, i.e. a second order critical point at zero coupling. It is therefore necessary to map out the phase structure of the theory and find the order of the critical points. Near the fixed point the lattice results are to be compared with weak coupling expansions to check if they scale according to the predictions of the renormalization group.

The internal energy, E = the expectation value of an elementary plaquette for SU(N) gauge theories, can be used as a probe to study the phase structure of the system. The presence of hysteresis in the heating versus cooling curves shows that the the theory has two distinct phases. There is a discontinuity in E at a first order phase transition. Points of second order transitions have no discontinuities, their trademark being a 'critical slowing down' accompanied by large fluctuations due to a diverging correlation length. To illustrate the dependence on the dimensionality of space-time and the gauge group, three models are considered in Fig.(2.1)[8]. The 5-dimensional SU(2) and the 4-dimensional SO(2) = U(1) theories show hysteresis and there exist two phases, confined and unconfined. The transition is first order for the SU(2) theory and second order for the U(1), with Q.E.D. being in an unconfined phase. The plot for SU(2) in four dimensions shows no discontinuity, and is believed to be in the confining phase. The behavior for SU(3) is similar, showing the critical nature of 4 dimensions for non-abelian gauge theories. One other remarkable point is the rapid crossover from the weak coupling to the strong coupling behavior. These results for SU(2) have been reproduced by us.

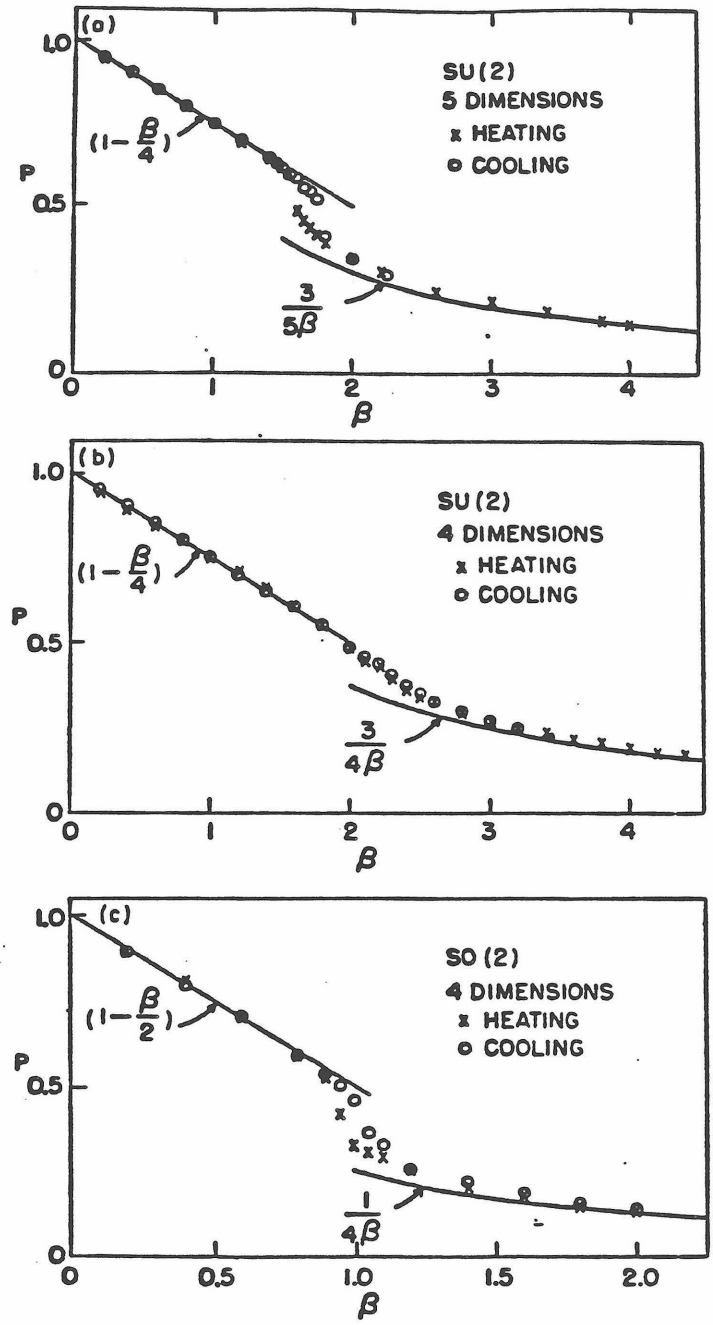

Figure 2.1: Thermal cycles to check for hysteresis[8].

The criterion for a theory to be confining is that at large distances the inter-quark potential grows linearly with the separation. Since the energy required to separate a quark and an anti-quark grows linearly, at a certain

separation it is energetically favorable to create a $q\bar{q}$ pair and form mesons. Thus color is confined. If we turn off the pair creation by considering infinitely heavy classical quarks, then the interaction term $\int A_\mu \cdot J_\mu$ reduces to a path-ordered line integral of the gauge field along the world line of the charges

$$\int DA \exp\left[-\beta S_G + \int d^4x\, A_\mu \cdot J_\mu\right] = \int DA[\, e^{-\beta S_G + P\int A_\mu dx^\mu}\,]$$

$$= \langle e^{P\int A_\mu dx^\mu} \rangle \,|_{pure\ gauge} \,. \qquad (2.3.1)$$

The last term is nothing other than the expectation value of a Wilson loop. Thus the extra action due to a $q\bar{q}$ pair created at some space-time point, separated to a distance R and held there for a long time T before being allowed to annihilate is given by the expectation value of a rectangular Wilson loop $W(R,T)$. For a potential with a linear term that dominates at large distances ie, $V(r)\to\sigma r$, we expect

$$\langle W(R,T)\rangle \sim e^{-\sigma RT - b(R+T) - d}. \qquad (2.3.2)$$

The constant term comes from the presence of sharp corners while the perimeter dependence is due to the self interaction. The latter is also the free energy of a quark which in the confined phase is infinite. Thus the Wilson loop is an order parameter with an area (perimeter) behavior implying a confined (unconfined) phase. In the confining phase the string tension, σ, controls the behavior of large loops and can be isolated by considering the quantities

$$X(i,j) = -\ln\left[\frac{W(i,j)\,W(i-1,j-1)}{W(i,j-1)\,W(i-1,j)}\right]$$

$$\cong \sigma a^2. \qquad (2.3.3)$$

If we renormalize the theory keeping σ fixed, then in the weak coupling limit the renormalization group predicts its behavior in terms of the lattice scale Λ_L

$$\sigma = const\ \Lambda_L^2 \tag{2.3.4}$$

where we use the two loop definition

$$\Lambda_L a = \left[\frac{11g^2}{16\pi^2}\right]^{\frac{-51}{121}} e^{\frac{-8\pi^2}{11g^2}} \quad . \tag{2.3.5}$$

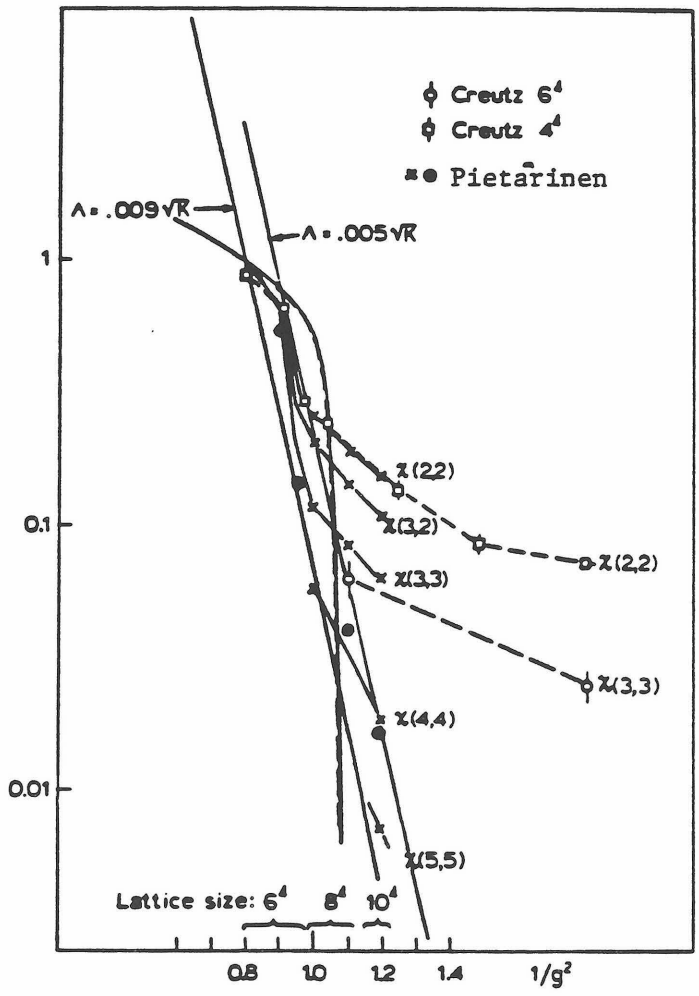

Figure 2.2: The plot of string tension X (i,j) versus $\frac{1}{g^2}$

Thus a plot of σa^2 versus $\frac{1}{g^2}$ will fix the constant in Eq.(2.3.4). This is shown in Fig.(2.2) for SU(3) and the result is[9]

$$\Lambda_L \cong \begin{bmatrix} 0.005 \\ 0.009 \end{bmatrix} \sqrt{\sigma} \tag{2.3.6}$$

The scales of the lattice and continuum theories are related by[10]

$$\frac{\Lambda_{mom}}{\Lambda_L} = 83.5 \tag{2.3.7}$$

and using the relation $\sigma = \frac{1}{2\pi\alpha}$, where $\alpha = 0.9 Gev^{-2}$ is the Regge slope, one finds that

$$\Lambda_{mom} \sim (170 \sim 300) Mev. \tag{2.3.8}$$

There are two sources of systematic errors that may significantly affect these numbers. 1) The Wilson loops used in the calculation are small and terms like $T \ln R$ have been neglected in Eq. (2.3.2). 2) the extrapolation using the renormalization group has been made from large values of g. To conclude, from these results one may only claim quantitative (up to factors of 5) confirmation that QCD is an asymptotically-free theory and is confining.

A related order parameter is the Wilson string defined as[11]

$$L(\vec{r}) = \frac{1}{N} Tr \exp\left[ig \int_0^\beta d\tau \, \frac{\vec{\lambda}}{2} \cdot \vec{A}_0(\vec{r},\tau) \right] \tag{2.3.9a}$$

which on the lattice becomes

$$L(\vec{r}) = \frac{1}{N} Tr \prod_{\tau=1}^{N_\tau} U_0(\vec{r},\tau). \tag{2.3.9b}$$

It is gauge invariant due to the periodic boundary conditions in the time

direction. The expectation value of L is related to the free energy, F_q,of a static quark as

$$< L > \sim e^{-\beta F_q} \tag{2.3.10}$$

For infinitely heavy quarks, the free energy of a single quark is devoid of content. On the other hand if its temperature dependence can be isolated and shown to be finite above some non-zero temperature and infinite below, then that would make it a bonafide order parameter to study confinement with. This has been done for the SU(2) theory[11], and the Monte Carlo simulations show a deconfining transition at a temperature of about 170 Mev. In addition, the correlation of two such strings measures the free energy of $q\ \bar{q}$ pair and can be used, along with Wilson loops, to measure the the string tension σ.

The next thing one can calculate for a pure gauge theory is the glue-ball spectrum. The logarithmic rate of fall-off of the 2-point correlation function for operators that couple the vacuum to definite glue-ball states is the mass-gap. The method is described in detail in section (3.3) so the results alone are discussed here. The qualitative features that emerge are that the states are massive and that the spectrum is dense. Quantitatively the results are poor. This is because the correlation function dies out in one or two steps for the range of g studied. In this case the mass-gap is estimated accurately only if one knows the exact operator that creates the desired state (see section (3.3)). Nevertheless the reported value for the 0^+ state in SU(3) from one step falloff is[12]

$$m(0^+) = (4.2 \pm .6)\, \Lambda_{mom} \tag{2.3.11}$$

The results for SU(2) are[13],

$$m(0^+) = (3.6 \pm .35)\, \Lambda_{mom} \tag{2.3.12a}$$

$$m(2^+) = (6.5\pm1.5)\,\Lambda_{mom}. \qquad (2.3.12b)$$

Here a large change, (25%), was observed between the first step and the second which shows that the isolation of the state is poor. Previous calculations [14] did not isolate the states at all so we do not report their results. To avoid the problem of a rapidly falling correlation function we describe a Hamiltonian variational method in section (4.2) that may yield better estimates for glue-ball masses. This method is currently being tested on SU(2) in 2+1 dimensions which has the same problem of a rapidly decaying correlation function.

There has been a lot of interest in modifying the Wilson action by adding other couplings. This has been fired by the discovery of a richer phase structure in the multi-coupling constant space[15]. In Fig. (2.3), the phase diagram for a variant of the SU(2) action, i.e.,

$$S_G = \beta(1-\frac{1}{2}TrS_\square) + \beta_A(1-\frac{1}{3}TrS_{\square A}) \qquad (2.3.13)$$

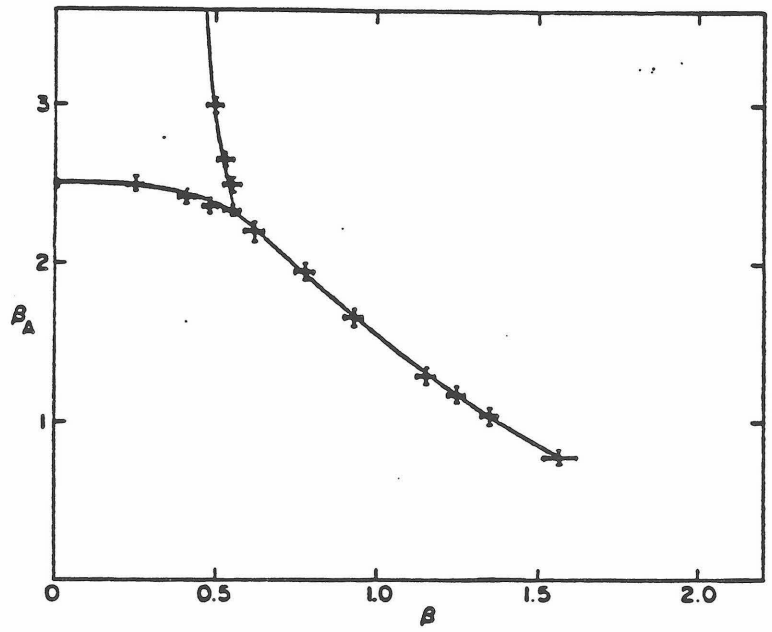

Figure 2.3: The phase diagram with the generalized action of Eq.(2.3.13)

is shown. β_A and S_{wA} are resp. the coupling and the group elements in the adjoint representation of SU(2). The first order transition line terminates before the SU(2) axis is reached. The value of β at which it would have intersected the SU(2) axis shows an anomalous bump in the specific heat[16], and is also the point of crossover from the weak coupling to the strong coupling behavior. In addition for SU(N, N>3), the line crosses the pure SU(N) axis[17]. It is our belief that while these singularities may be relevant to the applicability of strong coupling expansions, they do not affect the analysis unless they drive the region around g = 0 into the unconfined phase. However one has to be cognizant of their presence for they may strongly effect the scaling behavior in their vicinity[18]. So extrapolations to the continuum limit should be made from outside their range of influence. Also, such generalized actions may be useful in that they posses a stronger convergence to the continuum limit. This remains to be seen.

2.4: FERMION RESULTS IN THE QUENCHED APPROXIMATION

The two observables that immediately come to mind if the fermion correlation function can be calculated are

1) Hadron masses

2) Chiral behavior: What is the phase of the theory in the chiral limit? Spontaneously broken , $<\bar{\Psi}\Psi>\neq 0$, or not.

Predictably, the first Monte Carlo results were statements about these quantities. If results already exist then why has a full section(2.2) been devoted to the discussion of the existing difficulties in including fermions. The catch is that in the Quenched approximation the fermion determinant (see Eq.(2.1.18)) is set to 1 (in the loop expansion terms up to K^{12} only have been kept). Thus correlation functions are evaluated for pure gauge configurations. This approximation is not without some justification. Mass ratios of hadrons that do not have vacuum quantum numbers should not be affected by the absence of virtual quark loops if the following picture is correct. The color gauge fields that bind the quarks remain stringlike up to some length scale(hadron size) even in the presence of virtual $q\bar{q}$ pairs. The string tension, however changes. The real part decreases and it develops an imaginary part that is proportional to the decay width. Since we are interested in the masses, turning off the decay modes is in practice desirable. Also the real part of the string tension can be set to its true value by using a physical mass scale as input. In practice this is done by adjusting the lattice spacing so that either the calculated string tension gives the correct Regge slope, or that a hadron mass comes out right. Having so fixed the gauge coupling β, the second coupling constant K is then fixed by demanding that the mass of the pion be 140 Mev. This corresponds to fixing the bare quark mass. Note that the number of K parameters required is equal to

the number of different mass flavors. Having fixed these parameters the masses of all the other hadrons have no freedom left and are predictions of the theory.

The correlation function for non-strange mesons and baryons, described by their SU(4) wavefunctions, can be written in terms of the quark propagator Δ as

$$\langle \bar{\Psi}\,\Gamma\,\Psi |\; T^n \;| \bar{\Psi}\,\Gamma\,\Psi \rangle \;=\; \int D[U]\,\Delta(n,0,U)\,\Gamma\,\Delta(0,n,U)\,\Gamma \qquad (2.4.1)$$

$$\langle \bar{\Psi}\bar{\Psi}\bar{\Psi} |\; T^n \;| \Psi\Psi\Psi \rangle \;=\; \int D[U]\,\Delta(n,0,U)\,\Delta(n,0,U)\,\Delta(n,0,U) \qquad (2.4.2)$$

where we have suppressed the color, spin and flavor indices. Thus calculating the propagator and forming the appropriate products in the expectation values gives the masses of the states. The results published so far[19] show good agreement with the observed masses. The drawback of the quenched approximation and the subsequent data analysis is that an estimation of errors is as hard as solving the full theory. Therefore the good agreement in the numerical results may be taken as "proof" of that our model and understanding of hadronic masses is correct. A lot more work needs to be done before reliable and detailed answers are available.

The value of $\langle \bar{\Psi}_i \Psi_i \rangle$ in the limit of zero bare quark mass is an order parameter for the chiral behavior of the theory. The Wilson action, Eq.(2.1.14), with $r=0$ is best suited for this study since the chiral behavior is independent of the number of flavors. In this case the zero-mass limit is unambiguous, being given by $2ma \equiv \frac{1}{K} \to 0$. Hamber and Parisi[19] show that for the zero temperature theory the chiral limit is realized in the spontaneously broken phase. Kogut et. al.[20], by a similar calculation show that the symmetry is restored at a finite temperature and propose that the short range force responsible for it is independent of the confinement mechanism.

REFERENCES

[1] R. P. Feynman and A. Hibbs, *Quantum Mechanics* and *Path Integrals*, McGraw Hill, 1965.

[2] K. Wilson, Phy. Rev. D10 (1974) 2445.

[3] J. Kogut and L. Susskind, Phy. Rev. D11 (1975) 395.

[4] J. E. Hirsch, D. J. Scalapino, R. L. Sugar and R. Blankenbecler, Phys. Rev. Lett. 47 (1981) 1628.

O. Martin and S. Otto, CALT Preprint 68-901.

[5] D. Weingarten and D. Petcher, Phys. Lett 99B (1981) 333.

D. Weingarten, Indiana Univ. Preprint IUHET-69.

H. Hamber, Phys. Rev. D24 (1981) 951.

F. Fucito, E. Marinari, G. Parisi and C. Rebbi, Nucl. Phy. B180 [FS2] (1981) 369.

D. J. Scalapino and R. L. Sugar, Phy. Rev. Lett. 46 (1981) 519.

[6] N. Kawamoto, Nucl. Phys. B190[FS3] (1981) 617.

A. Hasenfratz and P. Hasenfratz, Phys. Lett. 104B (1981) 489.

C. B. Lang and H. Nicolai, Nucl. Phy. B200[FS4] (1982) 135.

[7] J. Kuti, I.T.P. Santa Barbara Preprint 81-151.

J. Hammersley and D. Handscomb, *Monte Carlo Methods*, John Wiley & Sons, New York, 1964, Chap. 7.

[8] M. Creutz, Phys. Rev. Lett. 43 (1979) 553.

M. Creutz, Phys. Rev. Lett. 45 (1980) 313.

[10] A. Hasenfratz and P. Hasenfratz, Phys. Lett. 93B (1980) 165.

[11] L. D. McLerran and B. Svetitsky, Phys. Lett. 98B (1981) 195.

J. Kuti, J. Polonyi and K. Szlachanyi, Phys. Lett. 98B (1981) 199.

[12] B. Berg and A. Billoire, CERN Preprint 3230 (1982).

[13] K. Ishikawa, M. Teper and G. Schierholz, DESY Preprint 81-089.

[14] B. Berg, Phys. Lett.. 97B (1980) 401.

G. Bhanot and C. Rebbi, Nucl. Phys. B180[FS2] (1981) 469.

[15] M. Creutz, BNL preprint 29840.

[16] B. Lautrup and M. Nauenberg, Phy. Rev. Lett. 45 (1980) 1755.

[17] I. G. Halliday and A. Schwimmer, Phys.Lett. 102B (1981) 327.

J. Greensite and B. Lautrup, Phy. Rev. Lett. 47 (1981) 9.

M. Creutz, Phy. Rev. Lett. 46 (1981) 1441.

H. Bohr and K. Moriarty, Phys.Lett. 104B (1981) 217.

[18] G. Bhanot and R. Dashen, IAS Preprint (1982).

[19] H. Hamber and G. Parisi, BNL Preprint 30170.

D. Weingarten, Indiana Univ. Preprint IUHET-69.

A. Hasenfratz, Z. Kunszt, P. Hasenfratz and C. B. Lang, CERN preprint 3220.

H. Hamber, E. Marinari, G. Parisi and C. Rebbi, BNL Preprint 30330.

[20] J. Kogut, M. Stone, H. W. Wyld, J. Shigemitsu, S. H. Shenker and D. K. Sinclair, Univ. of Illinois Preprint (1982) ILL -(TH)-82-5.

MONTE CARLO ESTIMATE OF THE MASS-GAP IN THE O(3) SIGMA MODEL

3.1: Introduction

In this chapter we investigate two Monte Carlo techniques for obtaining the mass-gap in a field theory. One is the long distance behavior of the 2-point correlation function using operators with definite quantum numbers. Second, we have developed a Hamiltonian variational Monte Carlo method which gives a bound on the mass-gap. Both these methods gave reliable results for the O(3) non-linear sigma model in 1+1 dimensions. This model was chosen because its critical behavior is similar to that of non-abelian gauge theories in 3+1 dimensions and also for reasons of tractability and limited computer power. These methods are general and applicable to any field theory, in particular to QCD.

The non-linear sigma models are defined by the following action

$$S = \frac{1}{2g} \int \nabla\vec{\varphi}\cdot\nabla\vec{\varphi}\; dx\; dt \qquad (3.1.1)$$

where $\vec{\varphi}$ is a N-component field, with the constraint

$$\vec{\varphi}\cdot\vec{\varphi} = 1 \quad . \qquad (3.1.2)$$

In 1+1 dimensions these theories are renormalizable and the global O(N) symmetry remains unbroken [2]. The spectrum is expected to be just an N-tuplet of massive particles. For $N \geq 3$ these theories are asymptotically free, and for $N = 3$ there exist instanton solutions (also true for QCD). The action (3.1.1) on a discrete spacetime lattice can be approximated as

$$S = \frac{-1}{g} \sum_m \left[\frac{\delta x}{\delta t}\, \vec{\varphi}_m\cdot\vec{\varphi}_{m+\hat{t}} + \frac{\delta t}{\delta x}\, \vec{\varphi}_m\cdot\vec{\varphi}_{m+\hat{x}} \right] \qquad (3.1.3)$$

where the constraint (3.1.2) has been used and an inessential constant dropped. δx and δt are the spacings in the space and time direction respectively. The global O(N) symmetry is preserved by this discretization. The Euclidean lattice theory is equivalent to the statistical mechanical problem of N component spins interacting via nearest neighbor couplings on a 2 dimensional lattice. This is the O(N) spin model. The phase structure of these models is well known [4]. The O(3) model has a critical point at $g = 0$, at which the correlation length diverges exponentially. The system has a non-zero mass-gap for all $g \neq 0$ and is therefore in the confining phase. To find the mass-gap for the field theory, we need to examine the behavior of the lattice theory in continuum limit ($\delta x = 0$, $\delta t = 0$). This shall be done using the renormalization group and is discussed in section(3.5).

The limit $\delta t \to 0$ in Eq. (3.1.3) leads to a quantum mechanical problem of a line of interacting spins. The corresponding Hamiltonian, as derived by Hamer, Kogut and Susskind [5], is

$$H = \frac{g}{2\,\delta x} \sum_m [J_m{}^2 - \gamma\, \vec{\varphi}_m \cdot \vec{\varphi}_{m+1}] \qquad (3.1.4a)$$

where

$$\gamma = \frac{2}{g^2} \qquad (3.1.4b)$$

and $\vec{J}_m$ is the N-component angular momentum operator at the site m. This Hamiltonian describes rotors on a N-sphere with nearest neighbor interactions. In the strong coupling limit (g large), γ is small and conventional perturbation theory may be used reliably. At $\gamma = 0$, the first excited state consists of a singly excited rotor of "spin 1", (N - tuplet), and this behavior must persist for some range of γ greater than 0. In fact it is expected that this is the case for all γ,

i.e. no level crossing occurs. Hamer, et al. [5] have calculated the mass-gap to sixth order in γ for the O(3) model. We have verified these strong coupling results by Monte Carlo simulation and have also found the mass-gap for the continuum field theory.

This chapter is organized as follows: The two methods are first derived and discussed, the Hamiltonian Monte Carlo variational technique in Section (3.2) and the 2-point (zero-momentum) correlation method in Section(3.3). A Lagrangian variational method for improving the accuracy of the 2-point correlation method is also described in section (3.3). The Monte Carlo method and some technical details of computer simulations are discussed in section (3.4) while the renormalization group analysis of the theory is presented in section (3.5). The results for these methods are given in Section (3.6) and the conclusions in section (3.7). Lastly, a detailed error analysis is included in section (3.8).

3.2: Hamiltonian Variational Method

The analytical solution for the ground state wavefunctional of field theories is usually not known and may be too complex for practical use. Monte Carlo simulation is an approximation scheme that can be used to generate field configurations that are distributed according to Ψ_0^2 on each time slice of the lattice. [1] Thus, the ground state expectation value of a physical observable $\mathcal{O}$ becomes a simple average over the generated configurations:

$$\int \mathcal{O}^2 \Psi_0^2 \rightarrow \sum \mathcal{O}^2. \tag{3.2.1}$$

[1] For a lattice of finite size in the time direction, the Monte Carlo generates the field variables on a given time slice according to the distribution Ψ_0^2 plus exponentially damped contributions from higher states. See reference [7]. There also are finite δt effects.

In the above, Θ should not be a differential operator acting on Ψ_0. We now describe a Monte Carlo variational method that gives an upper bound on the mass-gap [6].

Consider a Hamiltonian of the form

$$H = -\frac{1}{2}\nabla_x^2 + V(x). \tag{3.2.2}$$

Then the Raleigh-Ritz variational principle states that

$$E_1 \leq \frac{<\Psi_1^{Trial} \mid H \mid \Psi_1^{Trial}>}{<\Psi_1^{Trial} \mid \Psi_1^{Trial}>} \tag{3.2.3}$$

provided the trial wave function Ψ_1^{Trial} satisfies

$$<\Psi_1^{Trial} \mid \Psi_0> = 0 \tag{3.2.4}$$

where Ψ_0 is the exact ground state, i.e.,

$$[-\frac{1}{2}\nabla_x^2 + V(x)]\,\Psi_0 = E_0\,\Psi_0. \tag{3.2.5}$$

For Ψ_1^{Trial} construct the ansatz

$$\Psi_1^{Trial} = F(x)\,\Psi_0 \tag{3.2.6}$$

where F is a c-number function, and therefore commutes with the potential energy operator, $V(x)$. On substituting Ψ_1^{Trial} in Eq. (3.2.3), we eliminate the potential energy term by using Eq. (3.2.5). After an integration by parts, Eq. (3.2.3) can be rewritten as

$$E_1 - E_0 \leq \frac{1}{2}\,\frac{\int \nabla_x F^* \cdot \nabla_x F\,\Psi_0^2\,dx}{\int F^* F\,\Psi_0{}^2\,dx}. \tag{3.2.7}$$

The differential operator ∇_x acts only on $F(x)$. This is a consequence of the

product form of the ansatz.

An estimate for the mass-gap is now obtained by minimizing the right-hand side of Eq. (3.2.7). This is done by varying F subject to the constraint of Eq. (3.2.4). One way to realize this constraint is if Ψ_1^{Trial} has a different symmetry than the ground state. In particular, for the O(N) models, we take F to transform as an N-tuplet. Our motivation for the ansatz is the expectation that a simple F is sufficient to give a good bound. In the case of the simple harmonic oscillator, for example, a natural choice for F is "x" since Ψ_1^{Trial} will then automatically satisfy the constraint. This, of course, is the exact choice for F, and Eq. (3.2.7) becomes an equality. Similarly, for a scalar free field theory the exact F is the zero-momentum component of the field (the field being the analog of "x").

In the case of the O(N) models where the Hamiltonian is given by Eq. (3.1.4a), the bound is

$$E_1 - E_0 \leq \frac{g}{2\,\delta x} \frac{\int JF^* \cdot JF\ \Psi_0^2\, d[\varphi(x)]}{\int F^* F\ \Psi_0^2\, d[\varphi(x)]} \tag{3.2.8}$$

In the above, J is the N-component angular momentum operator that acts on F alone.

To minimize the right hand side of Eq. (3.2.7) we choose a set of trial functionals $F_1, F_2, \ldots, F_l$, and take

$$F^{Trial} = \alpha_1 F_1 + \alpha_2 F_2 + \cdots\cdots + \alpha_l F_l. \tag{3.2.9}$$

With this choice for F^{Trial}, and using Eq. (3.2.8) we get

$$E_1 - E_0 \leq \frac{g}{2\delta x} \frac{\sum \alpha_i^*\, G_{ij}\, \alpha_j}{\sum \alpha_i^*\, B_{ij}\, \alpha_j} \tag{3.2.10}$$

where G_{ij} and B_{ij} are given by

$$G_{ij} = \int JF_i^* \cdot JF_j \, \Psi_0^2 \tag{3.2.11a}$$

$$B_{ij} = \int F_i^* \cdot F_j \, \Psi_0^2. \tag{3.2.11b}$$

A key point of this method is that the functional integrals in Eq. (3.2.11) are evaluated using Eq. (3.2.1). One now minimizes the right-hand side of Eq.(3.2.10) subject to

$$\sum \alpha_i^* \, B_{ij} \, \alpha_j = 1 \tag{3.2.12}$$

which corresponds to the normalization

$$< \Psi_1^{Trial} \mid \Psi_1^{Trial} > = 1. \tag{3.2.13}$$

This is done by solving the generalized eigenvalue problem

$$\frac{g}{2\,\delta x} \sum G_{ij} \, \alpha_j = \varepsilon \sum B_{ij} \, \alpha_j \tag{3.2.14}$$

where ε is the Lagrange multiplier introduced by the constraint (3.2.12). The lowest eigenvalue, ε, is then the bound on the mass-gap. If the constraint (3.2.3) cannot be satisfied by a symmetry principle, one must include the functional

$$F_0 = 1 \tag{3.2.15}$$

in Eq. (3.2.9). The bound is then given by the second lowest eigenvalue of Eq. (3.2.14). We emphasize that the value so obtained is a bound only in the $\delta t \to 0$ limit. Also, F gives information about the wavefunctional of the single excitation spectrum.

3.3: 2-point Correlation Method

The operator that evolves a system from time τ to $(\tau + \delta\tau)$ is the Transfer Matrix T. Let $|k>$ be an eigenstate of T with the eigenvalue e^{-E_k}. Then the connected 2-point function for an operator Ω in the basis of these 'energy' eigenstates $|k>$ is

$$<\Omega(t+\tau)\cdot\Omega(t)> - <\Omega(t+\tau)>\cdot<\Omega(t)> = \sum_{k\neq 0} |<0|\Omega|k>|^2 \, e^{-(E_k - E_0)\tau} \qquad (3.3.1)$$

where the summation in k does not include the ground state and all states of energy lower than $\Omega\,|0>$. It is assumed that the operator Ω couples the given excited state to the ground state and is orthogonal to all the lower states. For large Euclidean time τ all states are exponentially damped and the one with the lowest eigenvalue dominates the sum in the correlation function

$$<\ldots> - <>\cdot<> \;\rightarrow\; |<0|\Omega|1>|^2 \; e^{-(E_1 - E_0)\tau}. \qquad (3.3.2)$$

The 2-point correlation function corresponds to the propagator in Minkowski time. The mass-gap is therefore given by its long distance behavior.

The above derivation supposed that E_1 was an isolated point in the spectrum. This is not true if there is a continuum of states above E_1 corresponding to non-zero momenta. A common choice for Ω in the O(N) models has been $\vec{\varphi}(x)$, the value of the field at a point. For this operator, the non-zero momentum states do contribute to the 2-point function, so a fit to $e^{-(E_1 - E_0)\tau}$ is inappropriate. This momentum smearing is significant even for Monte Carlo studies on a finite lattice. This effect increases as one approaches the critical point for then the density of states above E_1 grows, making the asymptotic behavior of Eq (3.3.2) even more difficult to determine. One must then measure the 2-point function at increasingly large time separations. This requires lattices that are large in the time direction, as well as very good statistics since the 2-point

function decays exponentially. The problem can be significantly reduced by choosing Ω so that the states directly above E_1 do not contribute. In order to do this, we take Ω to be a zero-momentum operator

$$\Omega = \tilde{\varphi}_0 = \int \vec{\varphi}(x,t)\, dx \tag{3.3.3}$$

which when discretized on the lattice becomes the total spin on a time slice. For the O(N) models, $\tilde{\varphi}_0$ is a very good choice, as the first excited state Ψ_1 is closely approximated by $\tilde{\varphi}_0\Psi_0$. This implies that the matrix element $< 0 \mid \Omega \mid 1 >$ in Eq. (3.3.1) is large compared to the matrix elements of the higher states.

To estimate the error due to the approximation in Eq.(3.3.2), we consider a simple case of when $\Omega\,|0>$ is a superposition of only two eigenstates of T, say $|a>$ and $|b>$

$$\Omega\,|0> \;=\; a\;|a> \;+\; b\;|b> \tag{3.3.4}$$

with $|a|^2 + |b|^2 = 1$ and $E_a < E_b$. Then

$$\frac{<0|\Omega\, T^N\, \Omega|0>}{<0|\Omega\, T^M\, \Omega|0>} \;=\; \frac{|a|^2\, e^{-E_a N} + |b|^2\, e^{-E_b N}}{|a|^2\, e^{-E_a M} + |b|^2\, e^{-E_b M}}$$

$$\sim\; e^{-E_a(N-M)}\left[1 + \frac{|b|^2}{|a|^2}\, e^{-(E_b-E_a)\,M}\,\left(\, e^{-(E_b-E_a)\,(N-M)} - 1\,\right)\right] \tag{3.3.5}$$

From Eq.(3.3.5), the error in the mass-gap is

$$\frac{\Delta m}{m} \;\sim\; \frac{1}{N-M}\,\frac{|b|^2}{|a|^2}\, e^{-(E_b-E_a)\,M}\,\left(\,1 - e^{-(E_b-E_a)\,(N-M)}\,\right) \tag{3.3.6}$$

where E_a is the true value. Thus the best estimate (smallest error) is gotten by taking M as large as possible while keeping $N-M$ small (1 step). We did not find any significant M dependence in the data and therefore concluded that Ω in Eq.(3.3.3) isolates the excited state to a very good approximation. For $M=0$ and

$N-M=1$, the error given by Eq.(3.3.6) depends only on the ratio b/a. Thus the first step is the most sensitive to contamination by higher states[3].

To fine-tune the operator Ω one can write it as a polynomial in the field variable φ with arbitrary coefficients $\{ a_i \}$

$$\Omega = a_1\varphi + a_3\varphi^3 + a_5\varphi^5 + ... \tag{3.3.7}$$

where all terms have the same symmetry and quantum numbers. The correlation function for the first step is then a matrix and the eigenvector corresponding to the lowest eigenvalue is the best estimate for the wave-function. The mass-gap should then be found by looking at the correlation of this state at large times τ. The problem of diagonalizing the matrix to get the lowest eigenvalue is the same as in the Hamiltonian Variational Method, however there is one very important difference between the two methods. The correlation function involves the Transfer Matrix and is therefore well defined for finite time-steps (Lagrangian formulation). In our analysis the 2-point correlation function, when fit to an exponential showed little if any relaxation [see Fig.1]. Consequently, we thought it unnecessary to implement this variational scheme.

In a Monte Carlo calculation one truncates the lattice in the time direction and imposes periodic boundary conditions to remove surface effects. For a lattice of periodicity P

$$\langle k \mid T^N \mid k \rangle = e^{-E_k N} + e^{-E_k (P-N)}. \tag{3.3.8}$$

Due to the second term, the correlation function starts deviating from an exponential fall-off for $N < P/2$. However the preceding analysis goes through unchanged provided that the second term in Eq.(3.3.8) is kept small by an appropriate choice of P and N. In general a fit should be made keeping both the terms.

3.4: The Theory of Monte Carlo Integration

The expectation value of physical observables $O[\varphi]$ have the generic form

$$\langle O \rangle = \frac{1}{\Xi} \int O[\varphi]\ e^{-S[\varphi]}\, D[\varphi] \tag{3.4.1}$$

where $S[\varphi]$ is the action, and Ξ is the generating functional written as a Path Integral. To evaluate this integral via Monte Carlo we approximate Eq.(3.4.1) by the sum

$$\langle O \rangle = \frac{1}{N} \sum_{i=1}^{N} O[\varphi^{(i)}] \tag{3.4.2}$$

over configurations $\{\varphi_{(i)}\}$, where the i^{th} configuration occurs with a probability

$$P[\varphi^{(i)}]\, D[\varphi^{(i)}] = \frac{1}{\Xi}\, e^{-S[\varphi^{(i)}]} D[\varphi^{(i)}] \tag{3.4.3}$$

The central point in Monte Carlo integration is to generate configurations with a distribution given by Eq.(3.4.3). This is done by setting up a Markov chain of configurations $\{\ \varphi^{(0)}, \varphi^{(1)}, \ldots\ldots\ \}$. These will converge to the desired distribution if the step from $\varphi^{(i)}$ to $\varphi^{(i+1)}$ is made with the probability $W[\varphi^{(i)} \to \varphi^{(i+1)}]$ such that the following conditions are satisfied:

$$W[\varphi^{(i)} \to \varphi^{(i+1)}] > 0$$

$$\int D[\varphi^{(i+1)}]\ W[\varphi^{(i)} \to \varphi^{(i+1)}] = 1 \qquad any\ \varphi^{(i)}$$

$$\int D[\varphi^{(i)}]\, P[\varphi^{(i)}]\ W[\varphi^{(i)} \to \varphi^{(i+1)}] = P[\varphi^{(i+1)}] \qquad any\ \varphi^{(i)} \tag{3.4.4}$$

The two standard choices for $W[\varphi^{(i)} \to \varphi^{(i+1)}]$ are referred to as the Metropolis and Heat Bath algorithms and are described below:

Metropolis algorithm[9]: The existing configuration is changed by an amount Δ, $\varphi^{(i)} \to \Delta * \varphi^{(i)} \equiv \chi$. Both Δ and "$*$" are symbolic and depend on the details of the theory. The only restrictions on Δ are,

i) Δ and its inverse Δ^{-1} occur with equal probability and

ii) starting from any given configuration $\{\varphi\}$ all other configurations can be reached by a repeated operation of Δ.

The new configuration χ is then kept with the probability

$$W[\varphi \to \chi] = 1 \qquad \text{if } S[\varphi] \geq S[\chi]$$

$$W[\varphi \to \chi] = \exp\left(S[\chi] - S[\varphi] \right) \quad \textit{otherwise.} \tag{3.4.5}$$

This method has the advantage that it is simple to implement. The value of the step size Δ controls the rate of convergence and has to be selected judiciously.

Heat Bath algorithm[1]: The probability, W, is taken to be the Boltzmann distribution

$$W[\varphi^{(i)} \to \varphi^{(i+1)}] = P[\varphi^{(i+1)}] = \exp\left[-S[\varphi^{(i+1)}]\right]. \tag{3.4.6}$$

This method requires that the integration over the measure (Haar for gauge theories) can be carried out to get $P[\varphi]$. Its advantage lies in a faster rate of convergence. The spin variables for the O(3) model were updated using the heat bath algorithm and we found it to be about 5 to 10 times faster than the corresponding Metropolis algorithm when sweep to sweep correlations are taken into account.

The field theories that we are interested in are local. This allows the Markov chain to be set up so that we update only one degree of freedom at each step. A consequence of this is that successive configurations are highly correlated and the phase space in the Path Integral is explored very slowly. A careful

study of the decorrelation time for our observables was made as a function of the lattice asymmetry and the correlation length. This is described in more detail in section (4.8). Another feature of algorithms that use a Markov chain is that the correct distribution e^{-S} is approached only asymptotically. The number of sweeps [1] needed to reach this distribution is called the thermalization time. This can be measured by determining when hot (random) and cold (ordered) starts converge to give the same average values for our observables. In practice, we assumed that the lattice had thermalized when the long distance part of the 2-point correlation function had stabilized.

The lattice can be used to study either the non-linear sigma model (i.e. the quantum field theory) or the spin system described by the Hamiltonian (Eq. (4.1.4a)). In the first case, one must find the mass-gap as given by our two methods in the limit, $\delta t \to 0, \delta x \to 0$. In the second case, the mass-gap of the quantum mechanical problem of a line of interacting spins can be found by taking the limit $\delta t \to 0$ for fixed δx. For this Quantum Mechanical problem a comparision of the two methods with known results from the strong coupling expansion is possible. To reach the Hamiltonian limit $\delta t \to 0$ we make the couplings anisotropic by taking $\delta t < \delta x$ in Eq. (4.1.3). The size of the lattice in the time direction is correspondingly increased by the same ratio to keep the total time constant. Since δt cannot be made exactly zero on the lattice, we have studied the convergence to the Hamiltonian limit.

The number of sweeps required to thermalize a lattice increases rapidly with the asymmetry. We reduced this time in the following way: An initial M × M lattice was brought into thermal equilibrium using symmetric couplings. The lattice was then converted to a 2M × M lattice (twice as large in time

[1] A sweep consists of having updated all the lattice sites once.

direction) by inserting an additional time slice between every adjacent pair, i^{th} and $(i+1)^{th}$, of the original lattice. The new variables were chosen by linearly interpolating between the old variables on the adjacent time slices:

$$\vec{\varphi}_{insert} = \frac{(\vec{\varphi}_i + \vec{\varphi}_{i+1})}{\| \vec{\varphi}_i + \vec{\varphi}_{i+1} \|} \tag{3.4.7}$$

The 2M × M lattice was then thermalized with δt half as much as it was on the M × M lattice. This procedure was repeated until the required asymmetry is reached. Since after each doubling the long distance behavior is preserved by the interpolation, the thermalization time for each stage is short. This trick substantially reduced the thermalization time.

All the calculations were performed on a VAX 11/780.

3.5: Continuum Limit and The Hamiltonian Formulation.

Wegner and Midgal [10] have conjectured that there are important similarities between 2-dimensional lattice spin systems and 4-dimensional gauge theories. So far, this conjecture has been very successful. The O(3) spin system and the non abelian gauge theories (for example SU(3)) have in common the following properties:

i) both theories are asymptotically free in the continuum. The two loop β-function for the O(3) model is [12]

$$\mu \frac{\partial g}{\partial \mu} = -\frac{1}{2\pi} g^2 - \frac{1}{(2\pi)^2} g^3 \ . \qquad (3.5.1)$$

Shenker and Tobochnik [4], using Monte Carlo Renormalization Group techniques on a square lattice, show that this weak coupling renormalization group (WCRG) behavior persists all the way up to $g \sim 0.7$.

ii) Both theories have a trivial critical point at $g = 0$. They stay disordered for all non-zero g and are characterized by an exponentially falling correlation function. Thus confinement and asymptotic freedom coexist in the same phase.

iii) There are instanton solutions for both theories. Recently several groups [13] have shown that block topological charge operators (which classify the topology of the field configurations on the lattice) have a well defined continuum limit. Extrapolations of their Monte Carlo results agree with the theoretical calculations in the continuum. Thus instanton configurations are sampled by our Monte Carlo procedure. However, it is not clear precisely what role they play in the dynamics of the theory; it is conjectured that they are responsible for the rapid cross over from the weak to the strong coupling behavior.

The lattice results are a function of the bare coupling constant g and the cutoff. We now discuss how one can obtain continuum (renormalized) values for

observables like the mass-gap from these lattice results. The β-function, Eq. (3.5.1), tells us how the bare coupling on the lattice depends on the cut off, and in analogy to QCD, one can define a Λ parameter that sets the mass scale of the theory. Shenker and Tobochnik [4] define the lattice Λ , Λ_L , as ($\beta \equiv \frac{1}{g}$)

$$\Lambda_L = \frac{1}{\delta x} (1+2\pi\beta) \exp(-2\pi\beta) \tag{3.5.2}$$

while Kogut and Shigemitsu [11] use the definition

$$\Lambda_L = \frac{1}{\delta x} (2\pi\beta) \exp(-2\pi\beta) \ . \tag{3.5.3}$$

This difference in the definition of Λ_L is due to a different choice for the constant when integrating the β-function in Eq.(3.5.1). The 2-loop definition of Λ_L has corrections of $O(\frac{1}{2\pi\beta})$ as reflected by the difference between Eqs. (3.5.2) and (3.5.3). We will consistently use Eq. (3.5.3) in the extrapolation to the continuum. It should therefore be remembered that there is a systematic error of ~ 10% in the continuum result because of the values of β we use. If the theory is renormalized keeping the mass-gap constant, then in the region where the WCRG is valid, the lattice mass-gap can be written as

$$\Delta m_L = C_L \Lambda_L = C\Lambda. \tag{3.5.4}$$

The value of C_L depends on the lattice parameters while C is a unique number for the continuum theory. We get C_L from our Monte Carlo calculations, and to find C the connection between Λ and Λ_L has been derived in chapter 4. The calculation was done using Pauli-Villars (PV) regularization for the continuum theory and the result for the symmetric lattice ($\delta t = \delta x$ as $\delta x \to 0$) is

$$\frac{\Lambda_{PV}}{\Lambda_L} = 27.21. \tag{3.5.5}$$

The Hamiltonian theory can be approximated on an asymmetric lattice if we introduce two couplings, g_t for the time (kinetic) part and g_x for the space (potential) part [11]. The lattice action then is

$$S = -\sum_m [\frac{\delta x}{v\, g_t\, \delta t} \vec{\Phi}_m \cdot \vec{\Phi}_{m+\vec{t}} + \frac{v\, \delta t}{g_x\, \delta x} \vec{\Phi}_m \cdot \vec{\Phi}_{m+\vec{x}}] \ . \tag{3.5.6}$$

We now make the choice

$$v^2 \frac{g_t}{g_x} = 1 \tag{3.5.7}$$

which implies that the length scales in the time and space direction are related by a variable speed of light v. Then

$$S = -\frac{1}{\sqrt{g_x g_t}} \sum_m [\frac{\delta x}{\delta t} \vec{\Phi}_m \cdot \vec{\Phi}_{m+\vec{t}} + \frac{\delta t}{\delta x} \vec{\Phi}_m \cdot \vec{\Phi}_{m+\vec{x}}] \tag{3.5.8}$$

is similar to Eq. (3.1.3) except that the coupling $g \to \sqrt{g_t g_x} \equiv g_H$. The corresponding Hamiltonian for the O(N) models, is

$$H = \frac{g_H}{2\,\delta x} \sqrt{\frac{g_t}{g_x}} \sum_m [\vec{J}_m^2 - \frac{2}{g_H^2} \vec{\Phi}_m \cdot \vec{\Phi}_{m+\vec{x}}] \tag{3.5.9}$$

where $\vec{J}_m^2$ is the angular momentum operator (see Eq. (3.6.5)). The speed of light v enters as an overall multiplicative factor. Therefore in addition to the connection between g_H and g_{cont}, or equivalently $\frac{\Lambda_{PV}}{\Lambda_L}$, we have to calculate $v \equiv \frac{1}{\sqrt{a}}$ as a function of the asymmetry $\frac{\delta x}{\delta t} \equiv n$. This calculation is done in chapter 4, and the results for O(3) are

$$\frac{\Lambda}{\Lambda_L} = \frac{8}{\sqrt{1+\frac{1}{n^2}}} \exp\left[n \tan^{-1}\frac{1}{n} + \frac{1}{n}\tan^{-1} n\right] \tag{3.5.10a}$$

and

$$\alpha = 1 + \frac{g_H}{\pi}\left[\frac{n}{\sqrt{\alpha}}\tan^{-1}\frac{\sqrt{\alpha}}{n} - \frac{\sqrt{\alpha}}{n}\tan^{-1}\frac{n}{\sqrt{\alpha}}\right]. \qquad (3.5.10b)$$

This variable speed of light $v \equiv \frac{1}{\sqrt{\alpha}}$ is also used to convert the correlation length measured in the time direction to the mass-gap expressed in units of the spatial lattice separation,

$$\delta m_{corr} = \frac{1}{\xi v} . \qquad (3.5.11)$$

Thus the mass-gap is scaled identically for the variational, Eq. (3.5.9), 2-point correlation, Eq. (3.5.11) and the strong coupling series methods. Therefore, if the lattice value agrees then the value in the continuum found by extrapolation will agree. The reason for introducing two couplings is that we shall use the WCRG to extrapolate the lattice results to the continuum from fairly large g, i.e. $g \sim 0.65$. If we could take the lattice large enough so that $g \simeq 0$ then $v \simeq 1$ and there would be no need to have two couplings provided the divergent parts in the renormalization of g_t and g_x are equal for $g_t = g_x$. This is true for these Spin models [see Eqs.(5.16)].

In the strong coupling region we are only interested in comparing the mass-gap from the variational, 2-point correlation function and the strong coupling series for a given lattice theory. It is therefore sufficient to take $g_t = g_x$ even though the strength of the kinetic versus the potential part has been scaled by the lattice asymmetry. The Monte Carlo results for the mass-gap using the methods of Sections [3.2] and [3.3] are presented next.

3.6: RESULTS

The 2-point Correlation Function Method.

In Section 2 we claimed that the use of the zero-momentum functional $\Omega = \sum\tilde{\varphi}(x)$ in the 2-point correlation function isolates the lowest excited state. Fig. [3.1] is a representative plot to emphasize the unambiguity in the exponential fall-off for this choice of the functional. The Monte Carlo results for the correlation length on a symmetric lattice are shown in Fig. [3.2] along with the 2-loop WCRG result

$$\frac{\xi}{\delta x} = B\,\frac{e^{2\pi\beta}}{1+2\pi\beta} \tag{3.6.1}$$

where we have measured B to be

$$B = 0.0085 \pm 0.0003 \ . \tag{3.6.2}$$

In the answer (3.6.2), the error quoted is statistical. The continuum mass-gap, using Eq. (3.5.5) and correcting for the difference in the definition of Λ_L between Eq. (3.5.2) and (3.5.3) is

$$\delta m = (4.8 \pm 0.2)\,\Lambda_{PV} \ . \tag{3.6.3}$$

Shenker and Tobochnik [4], by using the value for ξ found at $\beta = 1.42$ and on a 32 by 32 lattice, concluded that $B = 0.01 \pm 0.003$. They did not construct a zero-momentum functional and we believe that the difference in the results may partly be due to this. We have not investigated this possibility. Also, our data show that to assume WCRG behavior for $\beta < 1.475$ is unreliable, and there is $\simeq$ 10% systematic error in the continuum result if a lattice result for $1.42 \lesssim \beta \lesssim 1.475$ is extrapolated. In fact, for $\beta = 1.425$, we also get a larger value for B, i.e. 0.0091, than given in Eq. (3.6.2).

The results for the strong coupling region are presented later, along with the variational estimate.

The Monte Carlo Hamiltonian Variational Method.

The Monte Carlo variational mass-gap (MCVM) is obtained by minimizing the right hand side of

$$\Delta m \leq \frac{g_H}{2\,v\,\delta x}\,\frac{\Sigma \vec{J}F^{*}.\vec{J}F}{\Sigma\, F^{*}F} = \frac{g_H}{2\,v\,\delta x}\,\frac{\Sigma \alpha_i^{*} G_{ij}\alpha_j}{\Sigma \alpha_i^{*} B_{ij}\alpha_j} \quad . \tag{3.6.4}$$

On the symmetric lattice $g_t = g_x = g_H = g$ and $v = 1$. For the O(3) model

$$J_x = -i\,\vec{\varphi}_x \times \frac{\delta}{\delta \vec{\varphi}_x} \tag{3.6.5}$$

where the φ^a are the cartesian components of the N-tuplet of fields $\vec{\varphi}$. The explicit form of G_{ij} is

$$G_{ij} = \frac{\delta F_i^{*}}{\delta \varphi^a}\,\frac{\delta F_j}{\delta \varphi^a} - \varphi^a \frac{\delta F_i^{*}}{\delta \varphi^a}\,\varphi^\beta \frac{\delta F_j}{\delta \varphi^\beta} \quad . \tag{3.6.6}$$

The calculation of the matrix G_{ij} becomes increasingly time consuming as higher polynomials in φ are included in the functionals F_i. We therefore have not investigated polynomials higher than the third order. In the strong coupling region, $g > 0.8$ we take $g_t = g_x$, so that the Hamiltonian, Eq. (3.5.9), for a line of interacting spins is

$$H = \frac{g}{2\delta x} \sum_m \left[\, J_m^2 - \gamma\, \vec{\varphi}_m \cdot \vec{\varphi}_{m+\hat{x}} \right] \tag{3.6.7}$$

For small γ $\left(\equiv \frac{2}{g^2}\right)$ this corresponds to a line of rigid rotors with a moment of inertia $\frac{\delta x}{g}$ coupled by the interaction $\vec{\varphi}(x) \cdot \vec{\varphi}(x+1)$. The first excited state of

$\vec{J}^2$ is 3-fold degenerate [2] with quantum numbers J=1 and $J_z = \pm 1$ and 0. Similarly the continuum spectrum is supposed to be a triplet of $J=1$ states. We therefore chose the functionals F_i such that:

i) They transform like a vector under O(3) rotations. This condition insures that Ψ_1^{Trial} is orthogonal to the ground state Ψ_0.

ii) The excited state $\Psi_1^{Trial} = F\Psi_0$ is a state of zero momentum.

The simplest functional that satisfies this requirement is

$$F_0 = \sum_x \vec{\varphi}(x,t) \equiv \sum_x [\varphi_+ \vec{e}_+ + \varphi_- \vec{e}_- + \varphi_3 \vec{e}_3] \tag{3.6.8}$$

where $\vec{e}_\pm = \frac{1}{\sqrt{2}} (\vec{e}_1 \pm i\vec{e}_2)$ and $\vec{e}_3$ are the unit vectors in the internal O(3) space. To estimate the mass-gap, we chose in addition to the " naive " functional of Eq. (3.6.8) the following set of functionals with $J=1$ and $J_z=0$:

$$F_1 = \sum_x \vec{\varphi}(x) \cdot \vec{\varphi}(x+1) \varphi_3 (x+2) \tag{3.6.9a}$$

$$F_2 = \sum_x \vec{\varphi}(x) \cdot \vec{\varphi}(x+1) \sum_y \varphi_3(y) \tag{3.6.9b}$$

$$F_3 = \sum_x \vec{\varphi}(x) \cdot \vec{\varphi}(x+1)\, \varphi_3(x) \ . \tag{3.6.9c}$$

The restriction $J_z = 0$ (to be used in (3.6.8) also) is for convenience alone. We chose these functionals on the basis of the strong coupling analysis, which shows that the quantum mechanical excitations are local. This set is by no means complete; nevertheless, we believe that a representative set is sufficient to give a good bound on the mass-gap.

The variational method assumes that time is a continuous parameter. On the lattice we generate the Monte Carlo configurations with δx and δt as

[2] The three states are $\varphi_+ |0\rangle$, $\varphi_- |0\rangle$ and $\varphi_3 |0\rangle$ where $\varphi_\pm = \varphi_1 \pm i\varphi_2$.

independent parameters in the action of Eq. (3.5.8). The ratio $\frac{\delta t}{\delta x}$ can then be made as small as necessary to simulate continuous time. We decreased this ratio until the mass-gap from all three methods - MC variational, MC 2-point correlation function and the strong coupling series - agree. This allows us to find the value of the parameter $\frac{\xi}{\delta t}$ for which the eigenstates of the lattice transfer matrix are a good approximation to those for the Hamiltonian. In Fig. [3.3] we plot the behavior of the MC mass-gap as a function of the asymmetry $\frac{\delta t}{\delta x}$ for β = 0.6 , 1. , and 1.2 . The mass-gap by the correlation method converges to the strong coupling result from above, while the MCVM exhibits a hump before converging. More shall be said about this hump when we discuss the weak coupling results in Table 1. A linear extrapolation of the results for β = 0.6 in Fig. [3.3] does not quite converge to the strong coupling value. It must be noted that there is a systematic error for small spatial lattices (4 points in this case) due to higher mass states, which has not been fully taken into account (see section 3.8). Since the discrepancy is only a few percent, we did not feel it necessary to do a more detailed investigation at this time. In Fig. [3.4] we compare the largest asymmetry MC results with the the strong coupling series and a (3,3) Pade extrapolant to it. On the basis of the requirement that the mass-gap from the MCVM and the correlation function agree we conclude that for the O(3) model one needs $\frac{\xi}{\delta t} > 30$ to approximate continuous time to better than 10%.

In the weak coupling region, $\beta > 1.4$, we expect the functionals to be varying smoothly over the lattice. Otherwise, the gradients in the Hamiltonian would make the estimate for the mass-gap large. The functionals should also have a well behaved continuum limit. We therefore consider functionals that are qualitatively different than those of Eq. (3.6.9). Let $\varphi_3(k) = \sum e^{ikx}\varphi_3(x)$ be a Fourier component of momentum k, then for the weak coupling functionals we make the

ansatz

$$F = a_0\varphi_3(0) + a_{ijk}\ \vec{\varphi}(i)\cdot\vec{\varphi}(j)\ \varphi_3(k) \qquad (3.6.10)$$

with $i + j = k$ to insure that Ψ_1^{Trial} is a state of zero momentum. The explicit value of momenta used for the set (i,j,k) were (0,0,0) , (0,1,-1) , (1,-1,0) , (1,1,-2) , (1,-2,1) , (1,2,-3) , (2,-2,0) , (2,-3,1) and (3,-1,-2). Quadratic terms in φ were not considered as the interaction term is an even polynomial in the fields and the states are eigenstates under $\varphi \to -\varphi$.

In Fig. [3.5], we plot the MCVM (on a symmetric lattice) using the ansatz in Eq. (3.6.10). The data are fit to the WCRG result

$$\delta m = \frac{C_{L_0}}{\delta x}\, 2\pi\beta\, e^{-2\pi\beta} \qquad (3.6.11a)$$

or

$$\delta m_1 = \frac{C_{L_1}}{\delta x}\, (1 + 2\pi\beta)\, e^{-2\pi\beta} \ . \qquad (3.6.11b)$$

The best fit values of C_{L_0} and C_{L_1} are (112.8 ± 2.) and (102.2 ± 2.) respectively. The continuum mass-gap, using Eq. (3.5.5) and (3.6.11a), is

$$\delta m = (4.14 \pm 0.07)\ \Lambda_{PV}\ , \qquad (3.6.12)$$

where the error quoted is statistical. In this analysis the correlation length varies from about 8 to 15 over the range of β studied. This does not satisfy our criterion for the applicability of the variational method on the lattice ,i.e. $\frac{\xi}{\delta t} > 30$. Also the fit to Eq.(3.6.11a) is not as good as for the correlation method. Comparing the answer from the two methods, the MCVM gives a 13% lower value on symmetric lattices.

β	$\frac{\delta x}{\delta t}$ Latt.size	δm_{var} ±	δm_{corr} ±	C^{var} ±	C^{corr} ±
1.425	1 32*32	0.115 0.002	0.141 0.006	3.65 0.07	4.48 0.2
1.425	2 64*32	0.122 0.004	0.136 0.005	3.48 0.11	3.88 0.14
1.425	4 128*32	0.109 0.004	0.112 0.007	3.49 0.13	3.57 0.22
1.45	1 32*32	0.103 0.002	0.125 0.007	3.76 0.08	4.56 0.26
1.45	4 128*32	0.103 0.007	0.107 0.007	3.79 0.26	3.94 0.25
1.525	1 64*64	0.0724 0.002	0.086 0.003	4.03 0.11	4.8 0.2
1.575	1 64*64	0.058 0.002	0.066 0.004	4.28 0.15	4.87 0.3

Table 1 :O(3): Extrapolation of the lattice mass-gap to the continuum using the WCRG.

We had earlier concluded that the variational method would give reliable results on a symmetric lattice only for $\xi > 30$. An alternative is to work on asymmetric lattices. For the present, rather than use larger symmetric lattices to approximate the Hamiltonian theory, we used up to a 4-times asymmetric lattice for $\beta = 1.425$ and 1.45, where $\frac{\xi}{\delta t} > 35$. The results for these values of β are collected in Table 1, and the renormalized value, C, has been corrected for the scale changes implied by Eqs.(3.5.10). Figure [3.6] shows the dependence of the lattice mass-gap on the asymmetry for $\beta = 1.425$ and $g_t = g_x$. The first striking feature is that the humps in the MCVM mass-gap and in the scale connection are at the same asymmetry and that the continuum result is independent of the asymmetry. The result from the correlation method is however not constant but decreases to the MCVM value. This is quite unexpected since the correlation method does not rely on taking δt small. The other feature is that the MCVM on a symmetric lattice is increasing with β even though it is independent of the asymmetry. There are two possible explanations:

1) The finite size effects on lattices of different asymmetry vary due to a change in the correlation length. This would affect the 2-point correlation method more than the Hamiltonian variational.

2) The coupling is not small enough for the WCRG to be applicable. This had been concluded earlier and from Figs.[3.2,3.5] we see that the systematic errors due to this would underestimate the mass-gap. However, if one just looks at the MCVM at fixed β then the results suggest scaling. Kogut and Shigemitsu [11], using a (3,3) Pade extrapolation of the 6^{th} order strong coupling Hamiltonian series got a value $C_{cont} = 3.4 \pm 0.3$. Since the Pade approximant breaks down somewhere between $1{\cdot}4 < \beta < 1{\cdot}44$, they extrapolated from around β=1.425. Their result is consistent with our MCVM for the same coupling. From this we conclude that one has to very careful in deciding when the theory begins to

β	$\frac{\delta x}{\delta t}$ Latt.size	δm_{naive} ±	δm_{WC} ±	δm_{SC} ±	$\frac{1}{\xi} = \delta m_{corr}$ ±	δm_{Pade}
0.6	16 64*4	1.345 0.03	1.34 0.03	1.34 0.03	1.422 0.01	1.28
1.0	8 64*8	0.475 0.01	0.46 0.01	0.46 0.01	0.49 0.01	0.428
1.2	8 128*16	0.26 0.016	0.248 0.015	0.247 0.015	0.25 0.01	0.216
1.425	4 128*32	0.118 0.01	0.109 0.007	0.108 0.01	0.112 0.007	0.111
1.45	4 128*32	0.112 0.01	0.102 0.007	0.102 0.01	0.107 0.007	0.109

Table 2 :O(3): The comparison of the variational mass-gap (in units of δx) for the naive functional alone, with the values obtained when the WC and SC functionals are included. The three values are for the same data and the errors quoted are statistical. The mass-gap estimates from the correlation method and the strong coupling series are also included. Here $g_t = g_x$.

scale according to the WCRG. In future we propose to check whether the dependence of the correlation mass-gap on the asymmetry goes away at larger β.

In Table 2, we compare the effect of adding the local strong coupling functionals (SC), Eq. (3.6.9) and the weak coupling functionals (WC), Eq. (3.6.10), to the "naive" functional, Eq. (3.6.10), for identical runs on asymmetric lattices. We find that the SC and also the WC functionals lower the value of the mass-gap

by at most 10% over that given by the "naive" functional. This small effect may be due to our limited choice of the functionals or because Ψ_1^{Trial} is already a good approximation to Ψ_1 for the O(3) model. We believe that the latter is true, especially since the two qualitatively very different functionals behave almost identically. The other possibility is that as we approach the continuum limit, the number of operators grow (like the allowed momentum values), and keeping a fixed number of them lowers the mass-gap by a fixed percentage. A more detailed investigation is needed to settle this point and we hope to do this in the future.

3.7: CONCLUSIONS

The mass-gap from the two methods, 2-point correlation and variational, converges to the continuous time (Hamiltonian) limit as the lattice asymmetry $\frac{\delta x}{\delta t}$ is increased. When the coupling g is large, the Monte Carlo answers agree with the strong coupling series expansion. On the basis of this agreement we expect that the relevant parameter for approximating the $\delta t = 0$ limit is $\frac{\xi}{\delta t}$, and that for the O(3) model $\frac{\xi}{\delta t} > 30$ is required for 10 % accuracy. In the weak coupling region we have shown how to extrapolate results to the continuum using the renormalization group. At $\beta = 1.425$ and 1.45, we had expected a strong δt dependence in the Hamiltonian method. However the MCVM is quite independent of the asymmetry but increasing with β. We are therefore not yet in the scaling region, and the δt dependence may still be there. In the future we intend to resolve this issue by working at a smaller coupling.

It is interesting to note that for these spin models the first excited state is dominated by the 'naive' functional over the entire range of values of the

coupling studied. Thus the choice of the zero-momentum functional in the 2-point correlation method isolates the lowest excited state. This makes the estimate for the mass-gap very reliable. Using this method on symmetric lattices(Lagrangian formulation), we found the mass-gap for the continuum O(3) sigma model to be $\delta m = (4.8 \pm 0.2)\Lambda_{PV}$. We expect that for theories with a richer spectrum we can isolate states of definite quantum numbers by using functionals found by the variational methods of sections (3.2) and (3.3). To test this claim we propose to study SU(2) in 2+1 dimensions.

We do not understand why the mass-gap found by the correlation method changes with the asymmetry for β = 1.425 and 1.45. The likely explanation that we are not yet far out into the scaling region can be tested by working at smaller couplings. We hope to know the answer in the near future. In conclusion, while we have shown qualitative agreement of results, the necessity of extrapolating from large values of the coupling have left us with the several unanswered questions as mentioned above. This model has provided valuable experience and it is our hope that in theories where such detailed investigation is not possible, similar pitfalls can be avoided. A total of about 300 CPU hours on a VAX 11/780 were used in this calculation.

3.8: Error Analysis

3.8.1: Sweep to Sweep Correlation: The Statistics

The Monte Carlo methods described in section 3.3 do correctly generate configurations that are distributed according to $e^{-S[\varphi]}$. However, as each configuration depends on the previous one, they are *not* independent. The sweep to sweep correlation length, ξ_S, is proportional to the square of the ordinary spin-spin correlation length (as shown in section (3.8.2)) and gets large as when one approaches the continuum limit. We interpret ξ_S as a measure of the time it takes the Monte Carlo configurations to move through phase space. One must therefore take into account this correlation to get realistic error estimates.

Consider any observable $\Theta(s)$, where $s = 1, 2 \cdots S$ labels sweeps. Then one normally calculates a mean

$$\overline{\Theta} = \frac{1}{S} \sum_{s=1}^{S} \Theta(s) \tag{3.8.1}$$

and an error σ_Θ by

$$S\sigma_\Theta^2 = \frac{1}{S} \sum_{s=1}^{S} (\Theta(s) - \overline{\Theta})^2. \tag{3.8.2}$$

The correlation between the $\Theta(s)$'s does not affect Eq. (3.8.1), but it renders Eq. (3.8.2) invalid. If we denote Θ_{true} by the true mean of Θ (as opposed to the estimate $\overline{\Theta}$), one calculates

$$\sigma_\Theta^2 = < (\overline{\Theta} - \Theta_{true})^2 >$$

$$= \frac{1}{S^2} \sum_{s_1=1}^{S} \sum_{s_2=1}^{S} < (\Theta(s_1) - \Theta_{true})(\Theta(s_2) - \Theta_{true}) > \tag{3.8.3}$$

which reduces to (3.8.2) if $< (\Theta(s_1) - \Theta_{true})(\Theta(s_2) - \Theta_{true}) >$ is proportional to δ_{s_1,s_2}. In our case, this correlation coefficient is a function solely of $\delta s = |s_1 - s_2|$, and falls exponentially to zero as $|s_1 - s_2| \to \infty$. This is both predicted, as shown in section (3.8.2) and seen in our data. Put

$$c(\delta s) = < (\Theta(s_1) - \Theta_{true})(\Theta(s_2) - \Theta_{true}) >. \tag{3.8.4}$$

Then Eq. (3.8.2) becomes

$$S\sigma_\theta^2 = c(0)\left[1 + 2\sum_{\delta s = 1}^{\infty} \frac{c(\delta s)}{c(0)}\right] \tag{3.8.5}$$

where c(0) is estimated by Eq. (3.8.2), and

$$c(\delta s) \cong < (\Theta(s) - \bar{\Theta})(\Theta(s+\delta s) - \bar{\Theta}) >. \tag{3.8.6}$$

Eq. (3.8.5) predicts that roughly

$$S\sigma_\theta^2 \cong c(0)\,\xi_S \tag{3.8.7}$$

i.e. the errors are increased by $\sqrt{\xi_S}$ where $\frac{c(\xi_S)}{c(0)} = \frac{1}{e}$.

In practice, for most data points we had enough sweeps so that we could in fact find σ_θ by the distribution of the "block" average

$$\bar{\Theta}_k = \sum_{s=S_k+1}^{S_{k+1}} \Theta(s) \tag{3.8.8}$$

where

$$S_{k+1} - S_k \gg \xi_S \tag{3.8.9}$$

so that the individual $\bar{\Theta}_k$ are essentially uncorrelated.

3.8.2: Diffusion on the N-sphere

Here we give a simple theoretical model for the effects discussed phenomenologically in section(3.8.1). As an estimate of the number of sweeps required we have investigated the sweep to sweep correlation length ξ_S of the total spin $\vec{S}$ on the lattice,

$$\vec{S} = \frac{\sum_{x,t} \vec{\varphi}(x,t)}{|\sum_{x,t} \vec{\varphi}(x,t)|} . \tag{3.8.10}$$

We have found that such global observables move the slowest through phase space. If we assume that this vector $\vec{S}$ is doing a random walk on an N sphere, then the probability distribution $\rho(s,\vartheta_1,\ldots,\varphi)$ of $\vec{S}$ on the sphere is governed by the diffusion equation:

$$\frac{\partial \rho(s,\vartheta_1,\ldots,\varphi)}{\partial s} = K \vec{\nabla}^2 \rho(s,\vartheta_1,\ldots,\varphi) \tag{3.8.11}$$

where s labels sweeps and $\vec{S}$ is in the direction $(\vartheta_1,\ldots,\varphi)$ at sweep s. We now specialize to the O(3) model. The solution to Eq. (3.8.11) with a δ-function initial condition is

$$\rho(s,\vartheta,\varphi) = \sum_l \sqrt{\frac{2l+1}{4\pi}}\, Y_{l0}(\vartheta,\varphi)\, e^{-Kl(l+1)s} \tag{3.8.12}$$

where K is the diffusion constant. Then

$$< \vec{S}(s)\cdot\vec{S}(0) > = e^{-2Ks} = e^{\frac{-s}{\xi_s}}. \tag{3.8.13}$$

This diffusion constant will in general be a function of the algorithm used, the correlation length and the lattice asymmetry. Our Monte Carlo data show that this picture of random walk is correct and the sweep to sweep correlation length ξ_S is given by

β	$\frac{\delta x}{\delta t}$ (Latt.size)	ξ	ξ_s	$A = \frac{\xi_s \delta t^2}{\xi^2}$
0.6	4 (16*4)	0.6	6.2	1.1
0.6	8 (32*4)	0.67	28	1.0
0.6	16 (64*4)	0.703	105	1.2
0.6	32 (128*4)	0.725	472	0.9
1.2	2 (16*8)	2.94	42	1.2
1.2	4 (64*16)	3.7	231	1.05
1.2	8 (128*16)	3.85	993	1.05
1.425	1 (32*32)	7.1	97	1.9
1.425	2 (64*32)	7.41	264	1.2
1.425	4 (128*32)	9.09	1440	1.1
1.525	1 (64*64)	11.7	280	2.0
1.575	1 (64*64)	15.15	510	2.2

Table 3.3: Sweep to sweep correlation length of the total spin on the lattice. We find that $A \sim 1$ except for points on the symmetric lattice where the ratio is more like 2. If we had used $(1 \,/\, \delta m_{var})$ rather than ξ in this analysis then the ratio is ~ 1 for the symmetric lattice too.

$$\xi_S \equiv \frac{1}{2K} = A\,(\frac{\xi}{\delta t})^2 \,. \qquad (3.8.14)$$

The results for the O(3) model using the Heat Bath algorithm are given in Table 3 and we find that $A \simeq 1$. An analysis of this sort also provides a way of estimating the relative efficiencies of different algorithms by comparing the respective coefficients, A, of $(\frac{\xi}{\delta t})^2$.

3.8.3: Data Organization

The observables that we measure via Monte Carlo are all averages over the configurations generated. In the variational method, we accumulate the matrix elements

$$G_{i,j} = \nabla F_i^* \cdot \nabla F_j \quad \text{and} \quad B_{i,j} = F_i^* \cdot F_j \quad . \qquad (3.8.15)$$

Similarly for the correlation method, we accumulate

$$\Gamma(T) = \Omega(t+T) \cdot \Omega(t) \quad . \qquad (3.8.16)$$

The data were organized in blocks consisting of averages of the above observables over a certain number of sweeps. The precise number of sweeps per block was determined on basis of the sweep to sweep correlation length (discussed in sections(3.8.1)and(3.8.2)). Each block average constituted a data point and was used to determine the mass-gap and its statistical error. This averaging decreases the correlation of succesive data points in the sample.

As mentioned in section(3.8.1) the Monte Carlo generates configurations which are very correlated, consequently it is not useful to calculate observables every sweep. This is especially relevent if accumulating the averages dominates the CPU time used, as was true in our case. By performing several updates

between measurements, we balanced the update to calculation time without losing statistical accuracy. A typical value used in our calculation was 5 sweeps. A further optimization was implemented by calculating the matrix elements B_{ij} and G_{ij} on time slices sufficiently separated both within a sweep and from sweep to sweep. We were thus able to save CPU time without significant loss in accuracy.

3.8.4: Statistical Error in the Variational Bound

The value quoted for the bound is the smallest eigenvalue λ of

$$\frac{g}{2\,\delta x}\,\bar{G}_{ij}\alpha_j = \lambda\,\bar{B}_{ij}\alpha_j \quad . \tag{3.8.17}$$

where $\bar{G}_{ij}$ and $\bar{B}_{ij}$ are the matrix elements averaged over all the data. The corresponding eigenvector $\bar{F}$ is our best choice for F, so that

$$m = \frac{g}{2\,\delta x}\,\frac{\bar{F}^{*}\bar{G}\bar{F}}{\bar{F}^{*}\bar{B}\bar{F}} = \frac{\bar{N}}{\bar{D}} \quad . \tag{3.8.18}$$

We now take the projections, N_k and D_k, of the individual block matrices G^k and B^k in the direction $\bar{F}$,

$$\frac{g}{2\,\delta x}\,\frac{\bar{F}^{*}G^{k}\bar{F}}{\bar{F}^{*}B^{k}\bar{F}} = \frac{N^{k}}{D^{k}} \quad . \tag{3.8.19}$$

Let σ_N and σ_D be the errors in $\bar{N}$ and $\bar{D}$ evaluated from N^k and D^k. Here, if the blocks were not independent we averaged consecutive blocks until the sample became statistically uncorrelated. We found that $\sigma_N \sim 0$ for our Monte Carlo data, therefore

$$\frac{\sigma_m}{m} \sim \frac{\sigma_D}{\bar{D}} \quad . \tag{3.8.20}$$

In the above estimate, we have neglected the fluctuation in $\overline{F}$ which we expect to be small. Since the error in m is quadratic in the error in $\overline{F}$ ($\overline{F}$ being a solution of Eq.(3.8.17), this approximation is justified.

Another method for obtaining the statistical error on the mass-gap is to use the full probability distribution of the matrix elements $\overline{G}_{ij}$ and $\overline{B}_{ij}$. (The next section shows how we measured the corresponding error matrix for the case of the 2-point function). A sample of the matrices $G(n),B(n)$ can be generated via Monte Carlo according to the measured distribution. The lowest eigenvalue λ in Eq.(3.8.17) is then found for each case. The width of the probability distribution of λ gives the statistical error of the mass-gap. We attempted this analysis without taking into account the correlations between the different matrix elements. This often gave rise to negative eigenvalues in the distribution of λ, since the matrices $G(n)$ and $B(n)$ were no longer necessarily positive definite. In practice one can ignore these negative values, but the results obtained were not always reliable. We chose instead to estimate the error by using the previous method.

3.8.5: Statistical Error in the 2-point Function Mass Gap

We fit the measured 2-point function to an exponential over a range where we believe that the wrap-around and higher states have a minimal effect. This is done by a generalized χ^2 analysis because the points to be fit are highly correlated. Denote by $\Gamma(T)$ the average of $\Omega(t+T)\cdot\Omega(t)$ over all blocks of data, i.e.

$$\Gamma(T) = \frac{1}{N_{Tot}} \sum_k \gamma_k(T) \qquad (3.8.21)$$

where $\gamma_k(T)$ is the value of the 2-point function for block k. As the Γ's are averages, the central limit theorem applies, and for sufficiently many sweeps, they

become distributed as

$$P(\vec{\Gamma}) = e^{-(\vec{\Gamma}-\vec{\Gamma}_0)^T M^{-1} (\vec{\Gamma}-\vec{\Gamma}_0)} = e^{-\chi^2} \quad , \tag{3.8.22}$$

where $\vec{\Gamma}_0$ is the exact two point function, $\Gamma_0(T) = a_0 e^{-m_0 T}$. M is the error matrix:

$$M_{i,j} = < (\Gamma(T_i)-\Gamma_0(T_i))(\Gamma(T_j)-\Gamma_0(T_j)) > \tag{3.8.23}$$

where <...> denotes an average over hypothetical experiments (our Monte Carlo constituting one such experiment leading to one measurement of $\Gamma(T)$). If the blocks are uncorrelated, we can write

$$M_{i,j} = \frac{1}{N_{Tot}} \sum_k (\gamma_k(T_i)-\Gamma_0(T_i))(\gamma_k(T_j)-\Gamma_0(T_j)) \tag{3.8.24}$$

The exact parameters m_0 and a_0 in the 2-point function $\Gamma_0(T)$ are not known. In practice we can determine M to sufficient accuracy by using $\Gamma(T)$ instead of $\Gamma_0(T)$. There are two sources of problems in finding χ^2 using this expression for $M_{i,j}$. First, $\Gamma(T_i)$ and $\Gamma(T_{i+1})$ are very correlated. This makes all the matrix elements of M comparable in size, so that M has several small eigenvalues. Because it is M^{-1} that is used in the calculation of χ^2, this analysis is sensitive to the accuracy of these small eigenvalues. Second, if the block to block correlation is not small then averaging the blocks to make them independent leaves us with a rather small statistical sample. This makes the above problem of small eigenvalues even more severe. One *can* alternately determine $M_{i,j}$ from blocks that are statistically correlated by using a technique similar to that described in section(3.8.1), (see Eq. 3.8.5). Unfortunately, the corresponding corrections often violate the positivity requirement on M. Therefore the small eigenvalues cause a problem in this method as well.

The problem of the small eigenvalues of M was overcome in the following way. We observed that the eigenvectors of M with large eigenvalues corresponded to the lowest Fourier components of the 2-point function that are important in determining the slope. On the other hand the higher Fourier components had very small eigenvalues and contained no information relevant to the slope. We therefore removed the small eigenvalues and the corresponding components of the eigenvectors. The χ^2 analysis was then done on these degrees of freedom only. This must be kept in mind when calculating the reduced χ^2:

$$\chi^2_{red} = \frac{\chi^2}{\#\ degrees\ of\ freedom}$$

where the number of degrees of freedom is the number of eigenvalues kept in the analysis. The χ^2_{red} was then minimized by varying the parameters a_0 and m_0 in Eq. (3.8.22). The value of the mass-gap corresponds to the m_0 that gives the minimum χ^2_{red}, while the statistical error in the slope is the change in m_0 for χ^2_{red} to increase by 1 from this minimum. We found that the the error in the intercept a (the largest eigenvalue of M) was large, whereas the slope was determined with much better precision.

3.8.6: Systematic error in the 2-point function mass-gap

It is important to determine the sensitivity of the value of the slope to the choice of points used in the fit. Because we do not fit to a double exponential (to take into account the wrap-around due to periodic boundary conditions, Eq. (3.3.8)) and ignore contributions due to higher states (see section (3.3)), the value of the slope is subject to a systematic error depending on the points chosen. To analyze this effect, we determined the slope when in addition to the points chosen for the best fit, points at smaller T, and then at larger T were

included. This gave us a high and low value for the slope. The systematic error was then calculated by supposing that the slope had a flat distribution between m_{high} and m_{low}. We found this systematic error to be small. Since the spectrum of O(N) models is simple, the operator Ω in the 2-point function isolated the first excited state with a fair accuracy. Also, the lattice was large enough for the affect of the wrap-around to be small. This in fact is our justification for not including the second (wrap-around) term in Eq. (3.3.8), and for using the slope rather than a single step at large distance to estimate the mass-gap. In theories where the excited states are not dominated by a single operator, the 2-point correlation function should be analyzed as discussed in section (3.3).

References

[1] M. Creutz, Phys. Rev. D 21, 2308 (1980)

K. Wilson, Cargese Lecture Notes (1979)

[2] S. Coleman, Comm. Math. Phys. 31, 259 (1973)

[3] R. P. Feynman, Private Communication.

[4] S. Shenker and J. Tobochnik, Phys. Rev. D 22, 4462 (1980)

[5] C. Hamer, J. Kogut and L. Susskind, Phys. Rev. D 19, 3091 (1979)

[6] R. P. Feynman, *Statistical Mechanics*, W. A. Benjamin, Inc. 1972, pg. 328-329

[7] M. Creutz and B. Freedman, Brookhaven preprint, BNL 28588 (1980)

[8] J. Kogut, Rev. Mod. Phys., Vol 51, 659 (1979)

[9] N. Metropolis et al., J. Chem. Phys. 21, 1089 (1953)

[10] F. Wegner,J. Math. Phys. 12, 2259 (1971)

A. A. Midgal, Zh. Eksp. Teor. Fiz. 69, 810 and 1457 (1975)

[11] J. Kogut, J. Shigemitsu, Nucl. Phys. B, Vol B190 [FS3], 365 (1981)

J. Kogut, J. Shigemitsu, D.K. Sinclair, Phy. Lett., Vol 100B, 316 (1981)

[12] A. M. Polyakov, Phys. Let. B 59, 79 (1975)

E. Brezin and J. Zinn-Justin, Phy. Rev. B 14 , 3110 (1976)

[13] B. Berg and M. Luscher, Nucl. Phy. B, Vol B190 [FS3],412 (1981)

B. Berg, CERN Preprint 3076 (1981)

G. Martinelli, R. Petronzio and M. A. Virasoro, CERN Preprint 3074 (1981)

Figure Captions

[1] The 2 point correlation function for the zero momentum functional $\vec{\Omega} = \sum \vec{\varphi}(x)$ on a 64×64 lattice. The error bars (- symbol) ignore correlations between points and between data blocks (see section (3.8.5)). For a lattice of fixed spatial size, the wrap-around effect increases rapidly with the correlation length and the asymmetry.

[2] The correlation length ξ vs β for a symmetric lattice. To get the LTRG result, $\xi = 0.0085 \frac{e^{2\pi\beta}}{1+2\pi\beta}$, the fit was made to the Monte Carlo points with $\beta \geq 1.475$. We used a 32×32 lattice for $\beta \leq 1.475$ and a 64×64 lattice for $\beta \geq 1.5$.

[3] The lattice mass-gap vs. the lattice asymmetry for 3 values of β, i.e. 0.6, 1.0, and 1.2, in the strong coupling region. All values have been calculated with $g_s = g_t$. The errors shown are statistical. For the correlation method, the systematic errors increase with the asymmetry.

[4] Comparison of the mass-gap from the 2 point correlation method (triangles), MCVM (circles) and the strong coupling series in the Hamiltonian limit. We have taken $g_s = g_t$ for this comparison.

[5] The MCVM on a symmetric lattice. The coefficient C in the LTRG result is the best fit for $\beta \geq 1.475$. $\frac{\xi}{\delta t}$ is not yet large enough for this variational estimate to be reliable.

[6] Mass-gap vs. asymmetry for $\beta = 1.425$. We have taken $g_s = g_t$ as in figure 8.

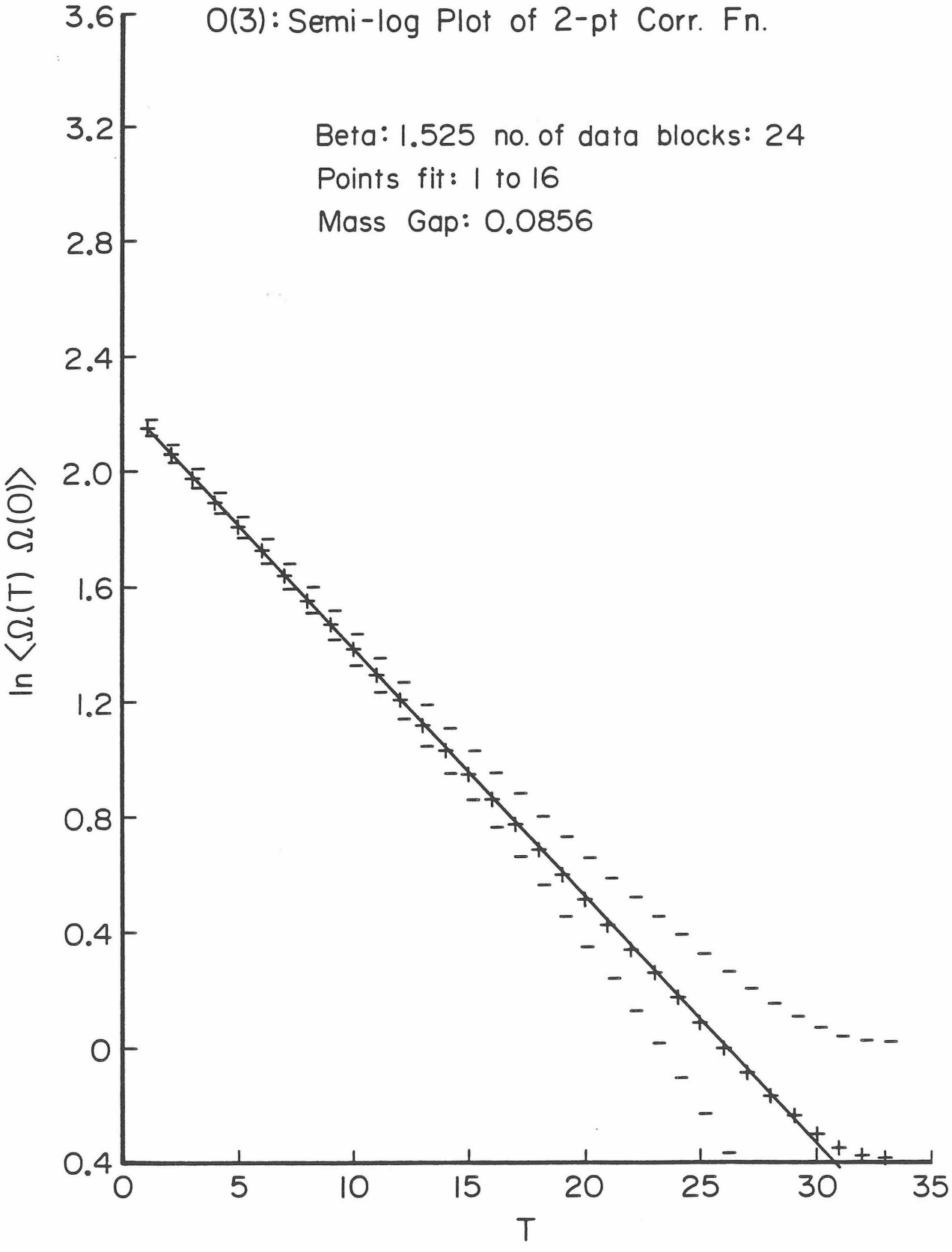
O(3): Semi-log Plot of 2-pt Corr. Fn.
Beta: 1.525 no. of data blocks: 24
Points fit: 1 to 16
Mass Gap: 0.0856
ln <Ω(T) Ω(0)>
T
3.6
3.2
2.8
2.4
2.0
1.6
1.2
0.8
0.4
0
0.4
0
5
10
15
20
25
30
35

Fig. 3.1

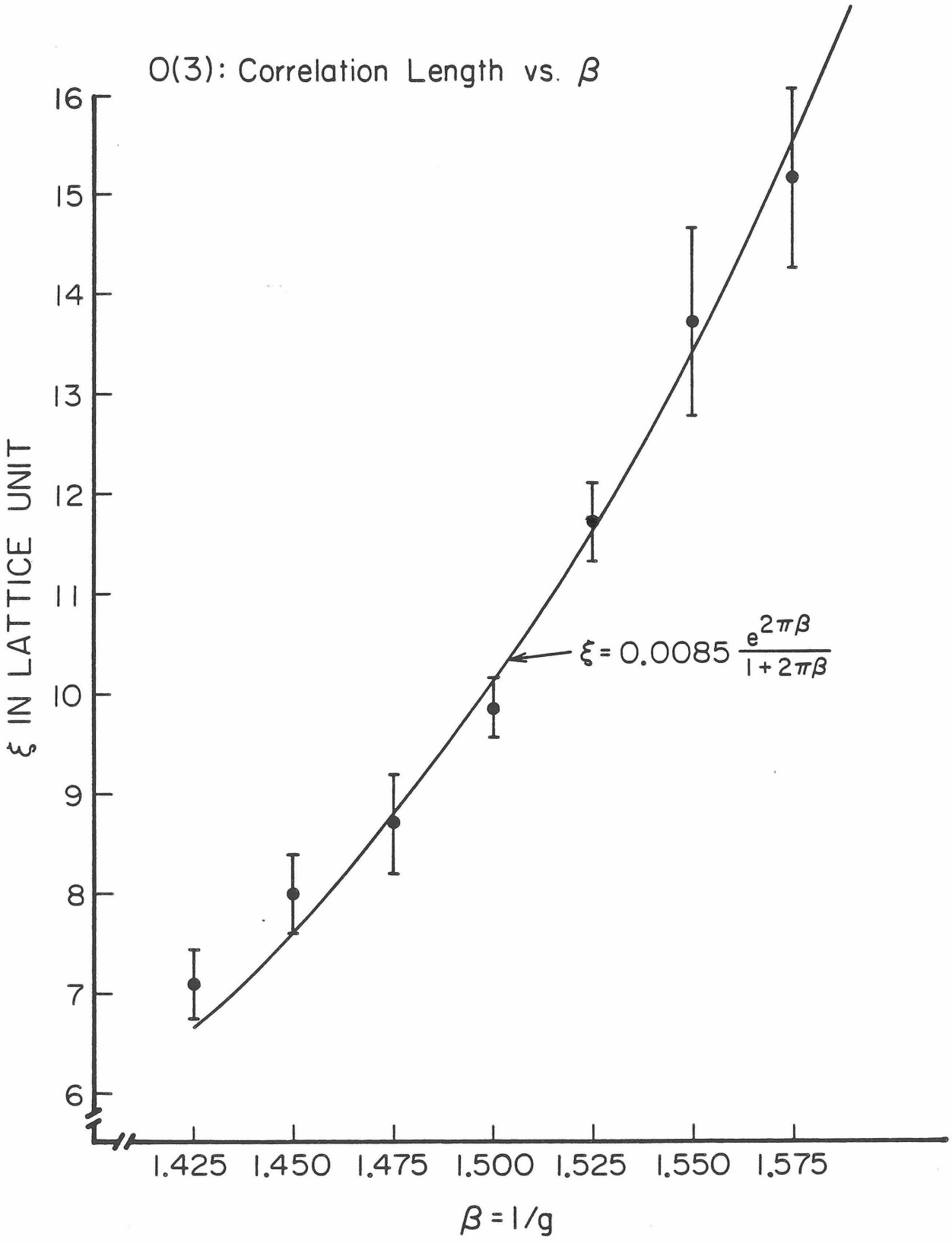
O(3): Correlation Length vs. β
ξ IN LATTICE UNIT
16
15
14
13
12
11
10
9
8
7
6
ξ = 0.0085 e^{2πβ} / (1 + 2πβ)
1.425
1.450
1.475
1.500
1.525
1.550
1.575
β = 1/g

Fig. 3.2

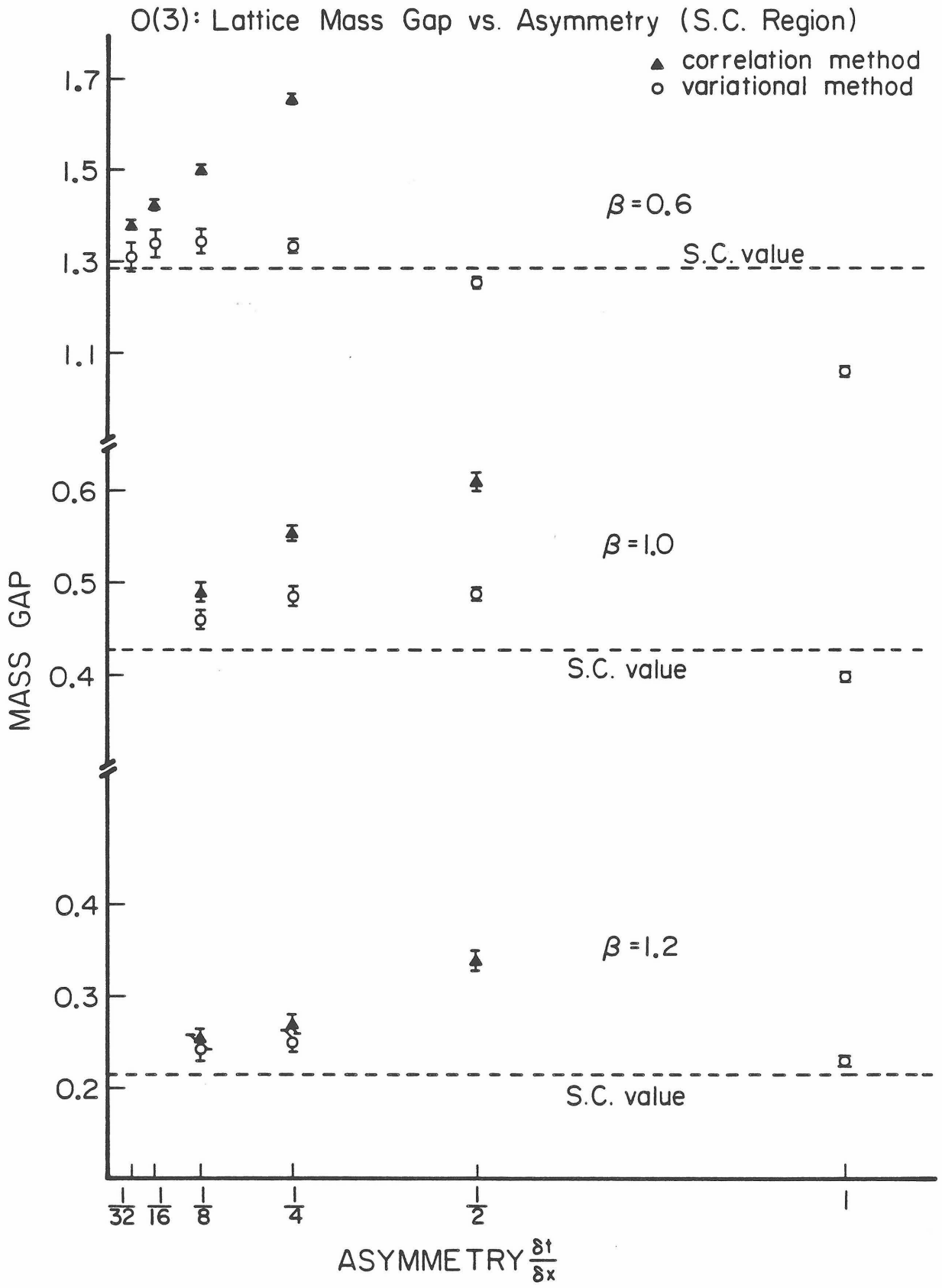
O(3): Lattice Mass Gap vs. Asymmetry (S.C. Region)
correlation method
variational method
MASS GAP
1.7
1.5
1.3
1.1
0.6
0.5
0.4
0.4
0.3
0.2
β = 0.6
S.C. value
β = 1.0
S.C. value
β = 1.2
S.C. value
1/32
1/16
1/8
1/4
1/2
1
ASYMMETRY δt/δx

Fig. 3.3

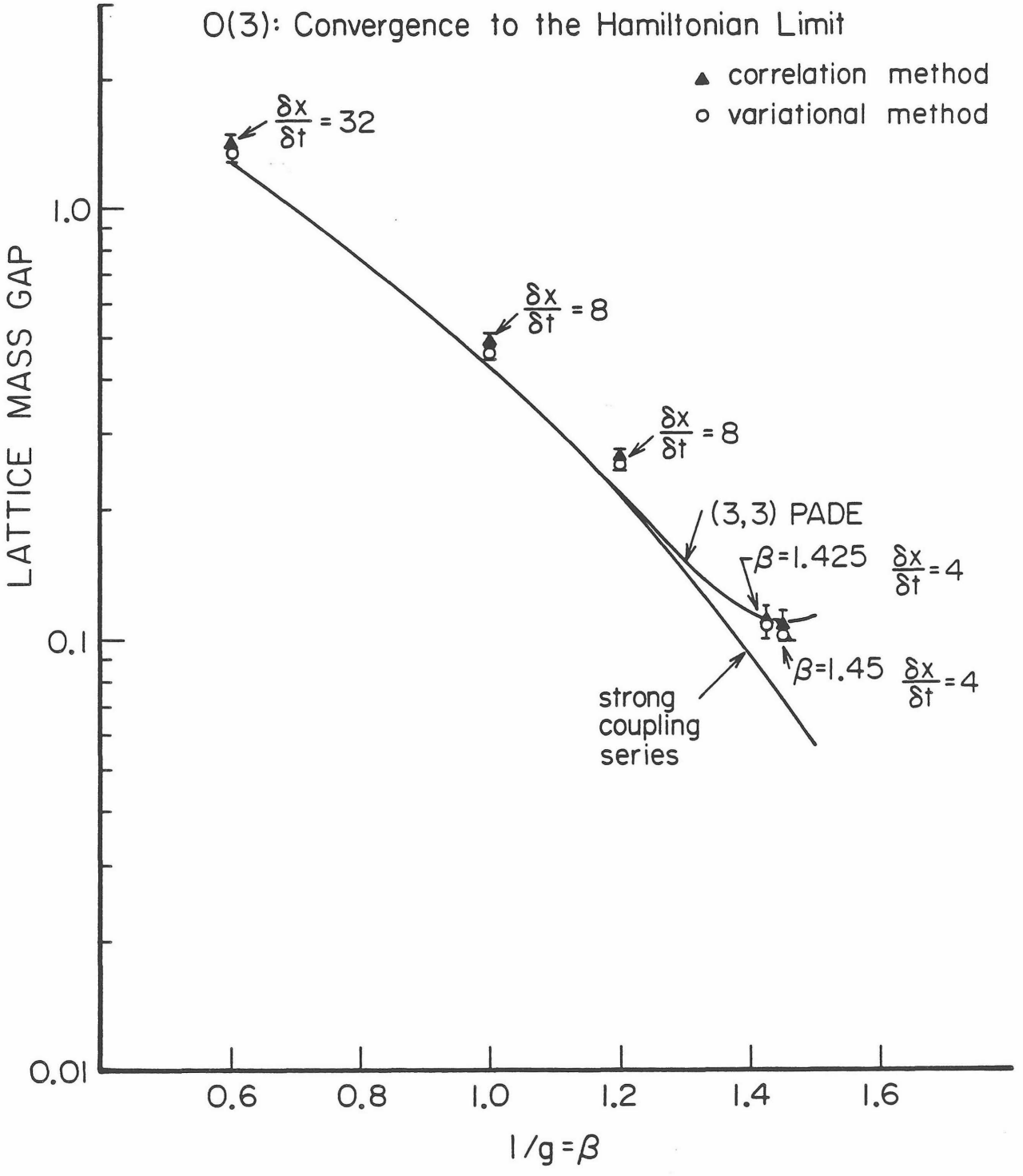
O(3): Convergence to the Hamiltonian Limit
▲ correlation method
o variational method
δx/δt = 32
δx/δt = 8
δx/δt = 8
(3,3) PADE
β=1.425 δx/δt=4
β=1.45 δx/δt=4
strong coupling series
LATTICE MASS GAP
1.0
0.1
0.01
0.6
0.8
1.0
1.2
1.4
1.6
1/g=β

Fig. 3.4

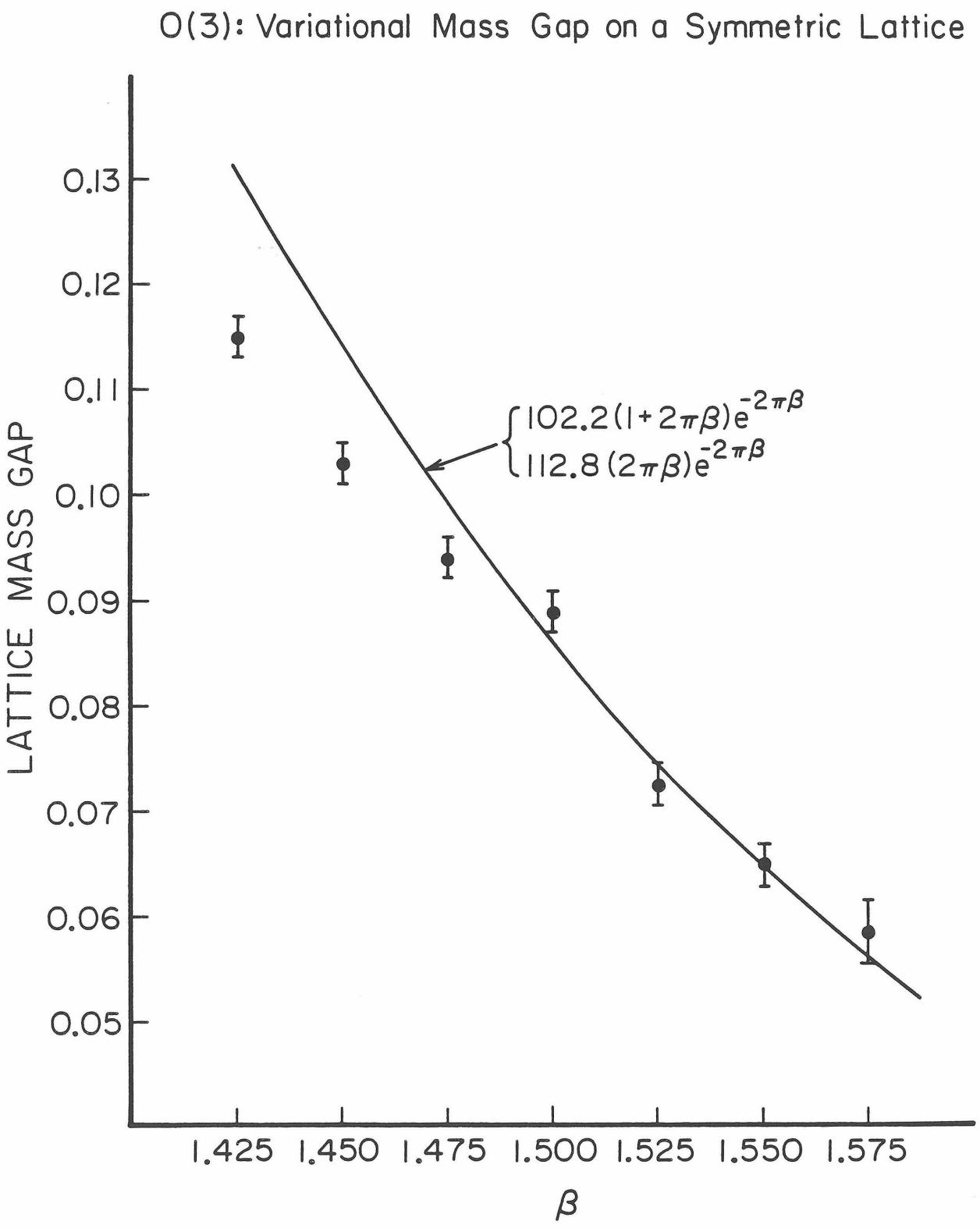
O(3): Variational Mass Gap on a Symmetric Lattice
LATTICE MASS GAP
0.13
0.12
0.11
0.10
0.09
0.08
0.07
0.06
0.05
$102.2(1+2\pi\beta)e^{-2\pi\beta}$
$112.8(2\pi\beta)e^{-2\pi\beta}$
1.425
1.450
1.475
1.500
1.525
1.550
1.575
β

Fig. 3.5

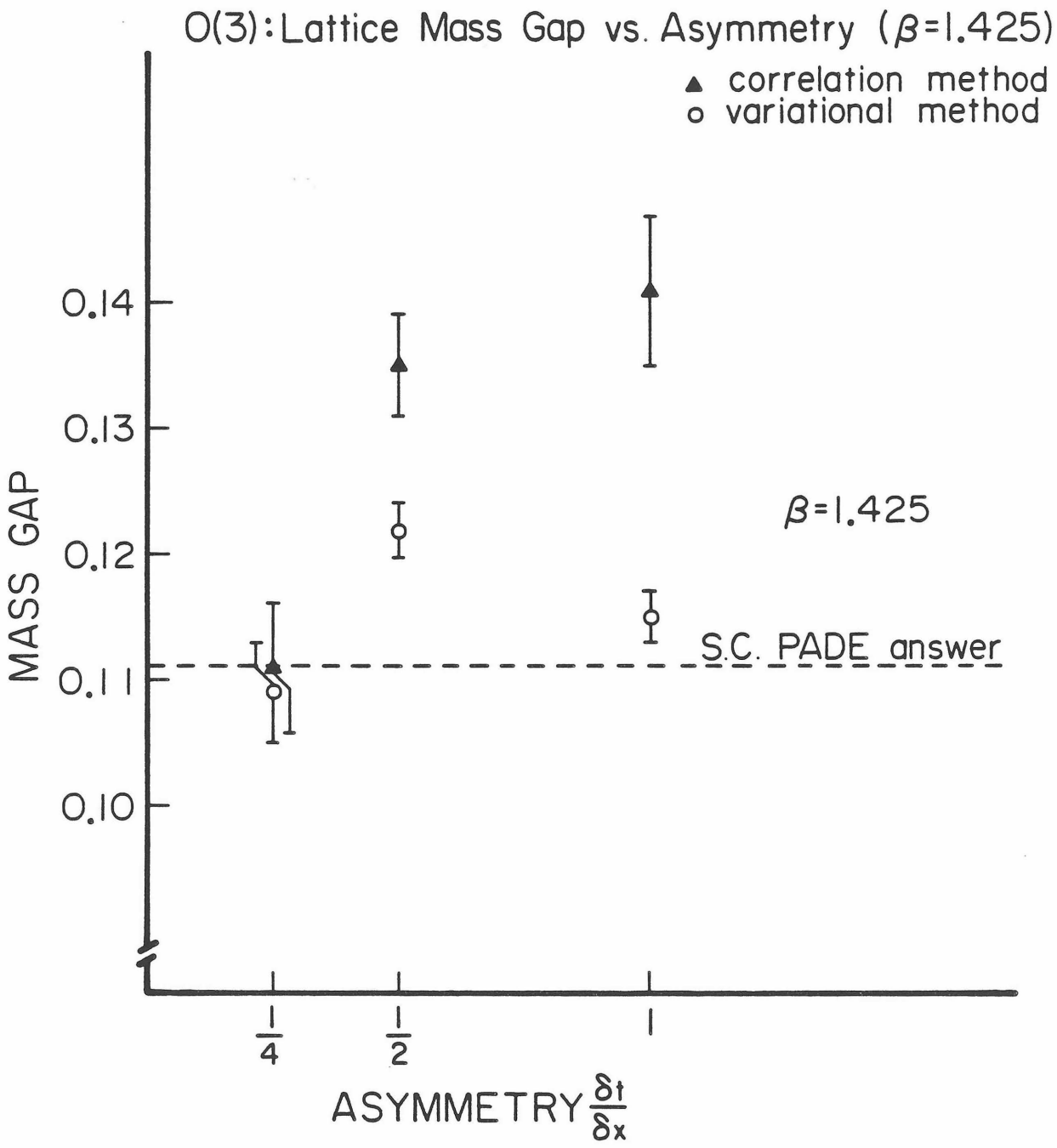
O(3): Lattice Mass Gap vs. Asymmetry (β=1.425)
▲ correlation method
o variational method
β=1.425
S.C. PADE answer
MASS GAP
0.14
0.13
0.12
0.11
0.10
1/4
1/2
1
ASYMMETRY δt/δx

Fig. 3.6

RELATION BETWEEN THE LATTICE AND CONTINUUM SCALES

In the continuum limit, the O(N) spin models (for N>2) in 1+1 dimensions are asymptotically-free field theories with no intrinsic mass scale. The dependence of the bare coupling-constant on the cutoff μ satisfies a simple renormalization group equation [1],

$$\mu \frac{\partial g}{\partial \mu} \equiv \beta(g) = -\frac{(N-2)}{2\pi} g^2 - \frac{(N-2)}{4\pi^2} g^3 + \cdots \tag{4.1}$$

To integrate this equation we have to specify the value of g at some reference momentum. The same is true of the renormalized coupling. However, instead of working with a coupling constant that depends on the renormalization point it is convenient to define a Λ-parameter that is a constant of integration in Eq.(4.1). This mass parameter Λ sets the scale for the renormalized theory and also specifies how $g(\mu)$ vanishes as $\mu \to \infty$. One possible definition is[4],

$$\ln\left(\frac{M}{\Lambda}\right) = \int_0^{g(M)} \frac{dg}{\beta(g)} - \int_0^{\infty} \frac{dg}{\beta_1(g)} \tag{4.2}$$

where $\beta_1(g)$ is the β -function truncated at 2 loops. This definition has the advantage of making the second term scheme independent. There still is an inherent scheme dependence in this perturbative definition of Λ. This is removed by the requirement that the physical renormalized coupling at some scale be equal in all regularization schemes. Thus

$$\frac{1}{g_{renorm}} = \frac{Z_L}{g_L} = \frac{Z_{cont}}{g_{cont}}. \tag{4.3}$$

To order g the renormalization constant $Z \simeq 1 + gR$, then using Eq.(4.2) we get

$$\frac{\Lambda_{cont}}{\Lambda_L} = M\, \delta x\, \exp\left[\frac{R(\delta x^{-1}) - R(M)}{\beta_0}\right]. \tag{4.4}$$

where Λ (Λ_L) and the cutoff M (δx^{-1}) correspond to the continuum (lattice) theory. Using the one loop expression for Z does not lead to an approximation, and the result in Eq.(4.4) is exact [3]. For the continuum theory, $R(M)$ using Pauli Villars regularization is[2],

$$R(M) = \frac{-(N-2)}{2\pi} \ln \frac{M}{\mu}. \tag{4.5}$$

To study the properties of a field theory from its lattice counterpart we need to look at its large distances behavior where the effects of the finite lattice spacing are negligible. This is most conveniently done near a critical point (2^{nd} *order*) where the correlation length diverges. However this limit can be taken with any fixed value of $\frac{\delta t}{\delta x}=n$. For each n there exists a different lattice theory. They all have the same continuum limit but correspond to a different regularization schemes. It is therefore necessary to derive the connection between Λ and Λ_L (ie. the renormalization constants) with the theory quantized on the given asymmetric lattice. This calculation is shown below for a lattice of arbitrary asymmetry n and the notation of chapter 3 is maintained.

The N-tuplet of fields is written as

$$(\Phi_i) \rightarrow (\Pi_i, \sigma). \tag{4.6}$$

The σ field is then integrated out using the constraint $\Phi\cdot\Phi = 1$ and the action in terms of the (N-1) component Π fields becomes

$$S = \frac{c\,\delta x\,\delta t}{2} \sum_{x,t} \Big(\frac{1}{g_t c^2 \delta t^2} \Big[(\partial_t \Pi)^2 + (\partial_t \sqrt{1-\Pi^2})^2 \Big] + \frac{1}{g_x \delta x^2} \Big[(\partial_x \Pi)^2 + (\partial_x \sqrt{1-\Pi^2})^2 \Big]. \tag{4.7}$$

And the generating functional for the theory is

$$\Xi = \int d\Pi \exp\left[-S - \frac{\delta^2(0)}{2}\int d^2x \ln(1-\Pi^2(x))\right]. \tag{4.8}$$

The delta function term comes from the Jacobian of the transformation. In order to regulate the infrared divergences, we add to the action a term

$$-m^2\,\sigma(x) \simeq \frac{m^2\Pi^2}{2} + \frac{m^2\,\Pi^4}{8}. \tag{4.9}$$

The action is then divided into the free part

$$S_0 = \frac{c\,\delta x\,\delta t}{2}\sum_{x,t}\left[\frac{1}{g_t c^2 \delta t^2}(\partial_t\Pi)^2 + \frac{1}{g_x \delta x^2}(\partial_x\Pi)^2 + \frac{1}{g_x}m^2\Pi^2\right], \tag{4.10}$$

and the interaction terms

$$S_I = \frac{c\,\delta x\,\delta t}{2}\sum_{x,t}\frac{1}{4}\left[\frac{1}{g_t c^2\delta t^2}\frac{(\partial_t\Pi)^2}{1-\Pi^2} + \frac{1}{g_x\delta x^2}\frac{(\partial_x\Pi)^2}{1-\Pi^2} + \frac{1}{gs}m^2(\Pi^2)^2\right]$$

$$- \frac{c\,\delta x\,\delta t}{2}\sum_{x,t}\Pi^2\delta^2(0) \tag{4.11}$$

where for brevity we have written m^2 for $m^2\delta x^2$. To make the notation simpler, the following change of variables is made

$$\Pi \to \Pi\sqrt{g_t}$$

$$\frac{\delta x}{c\,\delta t} = n$$

$$\frac{g_t}{g_x} = \alpha \quad ; \quad \sqrt{g_t g_x} = g_H. \tag{4.12}$$

S_0 and S_I can now be written as

$$S_0 = \frac{1}{2}\sum_{x,t}\left[\, n^2(\partial_t\Pi)^2 + \alpha\,(\partial_x\Pi)^2 + \alpha\, m^2\,\Pi^2\,\right] \tag{4.13a}$$

$$S_I \simeq \frac{g_H\sqrt{\alpha}}{2} \sum_{x,t} \frac{1}{4}\Big[n^2(\partial_t \Pi^2)^2 + \alpha(\partial_x \Pi^2)^2 + \alpha(m\ \Pi^2)^2 \Big] - \Pi^2\, \delta^2(0). \quad (4.13b)$$

The free field lattice propagator for each component, using S_0 given by Eq.(4.13a) is

$$G(x) = n \int_{-\pi}^{\pi} \frac{d^2k}{4\pi^2} \frac{e^{ikx}}{n^2(2-2\cos k_0) + \alpha(2-2\cos k_1 + m^2)}. \quad (4.14)$$

Because of the asymmetry of the lattice in space and time directions there are two renormalization constants Z_x and Z_t corresponding to g_x and g_t. These and the wave function renormalization constant Z are found by calculating the order g corrections to the propagator using standard techniques of perturbation theory. We find that[2],

$$\frac{Z}{Z_t} = 1 - g_t\ G(1,0)$$

$$\frac{Z}{Z_s} = 1 - g_t\ G(0,1)$$

$$\sqrt{Z} = 1 - g_t\ G(0,0) \quad (4.15)$$

which implies that

$$Z_t = 1 - g_t\ (N-2)\ G(0,0) + g_t\ [G(1,0)-G(0,0)] \quad (4.16a)$$

$$Z_x = 1 - g_t\ (N-2)\ G(0,0) + g_t\ [G(0,1)-G(0,0)]. \quad (4.16b)$$

The divergent part in Z_x and Z_t is equal to $O(g)$, which is required for the theory to be Lorentz invariant in the continuum limit. Also the differance in the finite part is the reason for having considered two couplings. This finite part is proportional to g and vanishes in the continuum limit leaving just one coupling. Thus to order g, the desired renormalization constant Z_H is given by Eqs. (4.16)

to be

$$Z_H = \sqrt{Z_t Z_x}$$

$$= 1 - g_t\,(N-2)\,G(0,0) + \frac{g_t}{2}\,[G(1,0) + G(0,1) - 2G(0,0)]$$

$$= 1 - g_H \sqrt{\alpha}\left[(N-2)\,G(0,0) + \frac{1}{2}\,[G(1,0) + G(0,1) - 2G(0,0)]\right]. \qquad (4.17)$$

Similarly the 'speed of light renormalization' is given by

$$\alpha_{renorm} = 1 = \alpha\frac{Z_x}{Z_t}$$

$$= \alpha\,[1 + g_t\,(\,G(1,0) + G(0,1) - 2G(0,0)\,)\,] \qquad (4.18)$$

The condition, $\alpha_{renorm}=1$, guarantees Lorentz invariance of the theory in the continuum limit. To get the desired relations, we now calculate $G(0,0)$ and $G(1)-G(0)$ starting from Eq.(4.14) for the free lattice propagator

$$G(0,0) = n\int_{-\pi}^{\pi}\frac{d^2k}{4\pi^2}\,\frac{1}{n^2(2-2\cos k_0) + (2-2\cos k_1 + m^2)} \qquad (4.19)$$

The integration over k_1 is straightforward, and making a change of variable, $\sin^2(\frac{k_0}{2}) = x$, we get

$$G(0,0) = \frac{1}{4\pi n}\int_0^1 dx\,\frac{1}{\left[x(1-x)(\frac{m^2}{z}+x)(\frac{4+m^2}{z}+x)\right]^{1/2}} \qquad (4.20)$$

where $z = \frac{4n^2}{\alpha}$. This is an elliptic integral. The solution is

$$G(0,0) = \frac{1}{\pi\sqrt{\alpha\,(1+\frac{m^2}{z})\,(4+m^2)}}\;K\left[\frac{4}{(1+\frac{m^2}{z})\,(4+m^2)}\right] \qquad (4.21)$$

which in limit $m \to 0$ reduces to

$$G(0,0) \sim \frac{1}{4\pi\sqrt{\alpha}} \ln\left[\frac{64}{m^2\,\delta x^2\,(1+\frac{\alpha}{n^2})}\right]. \tag{4.22}$$

The expression for $G(0,0) - (G(1,0)$ *or* $G(0,1))$ is easier to evaluate since it is infrared finite and therefore one can take the limit $m \to 0$ from the start. The result is

$$G(0,0)-G(0,1) = \frac{n}{\pi\alpha} \tan^{-1}\frac{\sqrt{\alpha}}{n} \tag{4.23a}$$

$$G(0,0)-G(1,0) = \frac{1}{\pi n} \tan^{-1}\frac{n}{\sqrt{\alpha}}. \tag{4.23b}$$

Substituting Eqs.(4.22) and (4.23) into Eq.(4.17) gives

$$Z_H = 1-(N-2)\,\frac{g_H}{4\pi} \ln\left[\frac{64}{m^2\,\delta x^2\,(1+\frac{\alpha}{n^2})}\right]$$

$$-\frac{g_H}{2\pi}\left[\frac{n}{\sqrt{\alpha}} \tan^{-1}\frac{\sqrt{\alpha}}{n} + \frac{\sqrt{\alpha}}{n} \tan^{-1}\frac{n}{\sqrt{\alpha}}\right]. \tag{4.24}$$

From Eq.(4.24) we can read off $R(\delta x^{-1})$ and using Eqs.(4.3) and (4.5) we get the desired result (choosing $m=\mu$)

$$\frac{\Lambda_{PV}}{\Lambda_L} = \frac{8}{\sqrt{1+\frac{1}{n^2}}} \exp\left[\frac{n \tan^{-1}\frac{1}{n} + \frac{1}{n}\tan^{-1}n}{N-2}\right] \tag{4.25}$$

where we have set $\alpha = 1$ since Λ is defined in the limit $g \to 0$. The two limiting forms, Hamiltonian and Lagrangian, for this connection are

$$\frac{\Lambda_{PV}}{\Lambda_L}\Big|_{n=\infty} = 8 \exp\left(\frac{1}{N-2}\right)$$

$$\frac{\Lambda_{PV}}{\Lambda_L}\Big|_{n=1} = \frac{8}{\sqrt{2}} \exp\left(\frac{\pi}{2(N-2)}\right) \tag{4.26}$$

These limiting forms have been calculated by Kogut and Shigemitsu [2]. Finally, using Eqs.(4.17), (4.22) and (4.23), we get

$$\alpha = 1 + \frac{g_H}{\pi}\left[\frac{n}{\sqrt{\alpha}} \tan^{-1}\frac{\sqrt{\alpha}}{n} - \frac{\sqrt{\alpha}}{n} \tan^{-1}\frac{n}{\sqrt{\alpha}}\right]. \tag{4.27}$$

The variable v, used in section[3.5], is related to α as

$$v = \sqrt{\frac{g_x}{g_t}} = \frac{1}{\sqrt{\alpha}} \tag{4.28}$$

The connection between the lattice and continuum scale, Eq.(4.25) is plotted in Fig. (4.1). It is surprising to find that the relationship does not go monotonically from the Euclidean to the Hamiltonian value. It exhibits a hump at an asymmetry of two. We had found a similar hump in the Hamiltonian Variational estimate of the mass-gap in section (3.6). It was shown there that the two humps are consistent and gave a value for the continuum mass-gap that was independent of the lattice asymmetry. However we do not at present understand why this is inconsistent with the correlation method. The behavior of α is shown in Fig. (4.2). To complete this discussion we tabulate below α and $\frac{\Lambda}{\Lambda_L}$, for the parameter values $\frac{1}{g_H}$ = 1.425 and 1.45 and the asymmetry n = 4.

β	$\frac{\delta x}{\delta t}$	α	v	$\frac{\Lambda}{\Lambda_L}$
1.425	4	1.14	0.9365	28.8
1.45	4	1.138	0.9375	28.8

REFERENCES

[1] A. M. Polyakov, Phys. Let. B59, (1975) 79.

E. Brezin and J. Zinn-Justin, Phy. Rev. B14, (1976) 3110.

[2] J. Kogut and J. Shigemitsu, Nucl. Phys. B, Vol B190[FS3], (1981) 365.

J. Kogut and J. Shigemitsu, Private communications.

G. Parisi, Phy. Lett. 92B, (1980) 133.

[3] W. Celmaster and R. Gonsalves, Phys. Rev. Lett., 42 (1979) 1435.

[4] P. Stevenson, Phys. Lett., 100B (1981) 61.

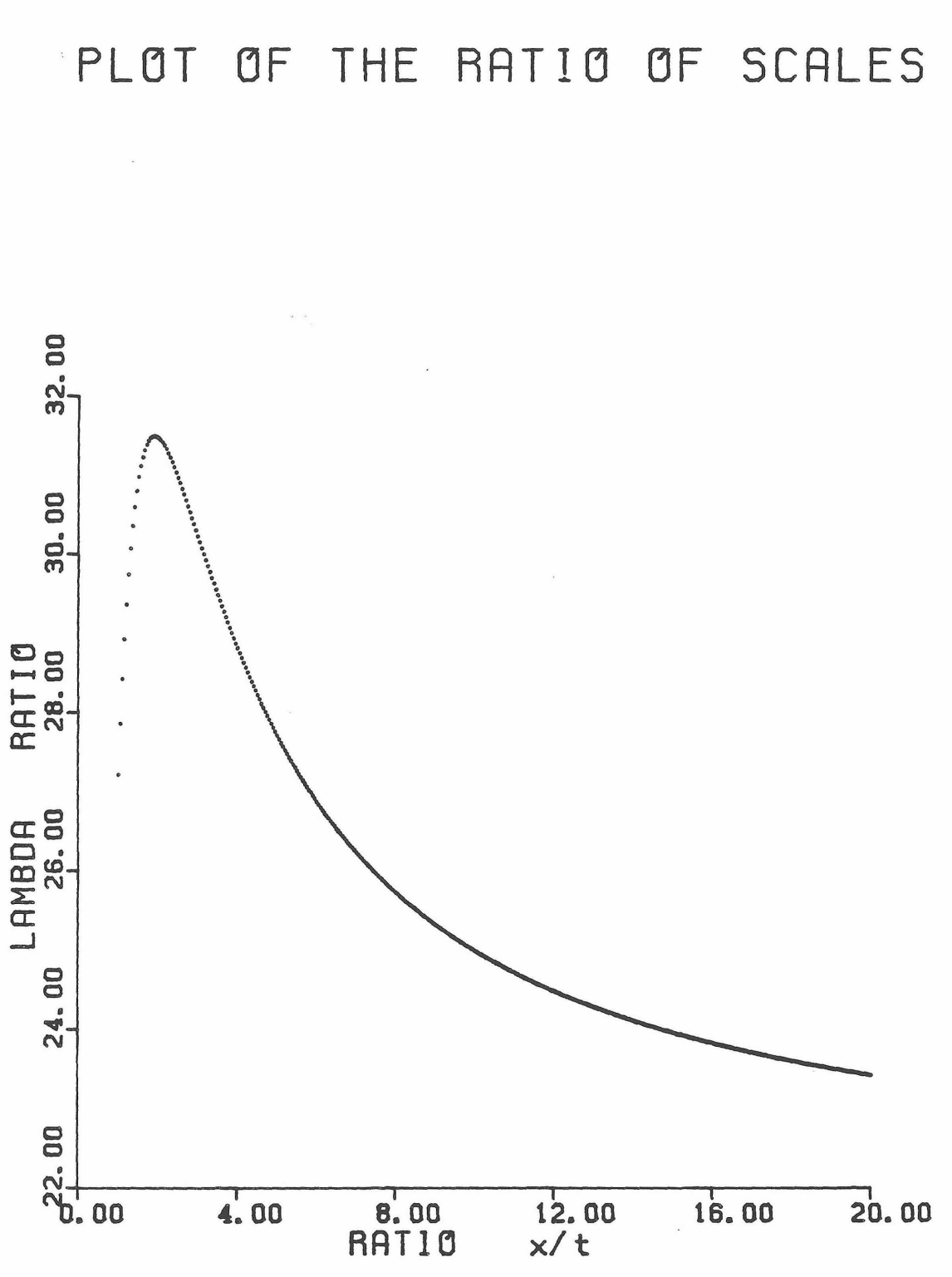
PLOT OF THE RATIO OF SCALES
LAMBDA RATIO
32.00
30.00
28.00
26.00
24.00
22.00
0.00
4.00
8.00
12.00
16.00
20.00
RATIO x/t

Fig. 4.1

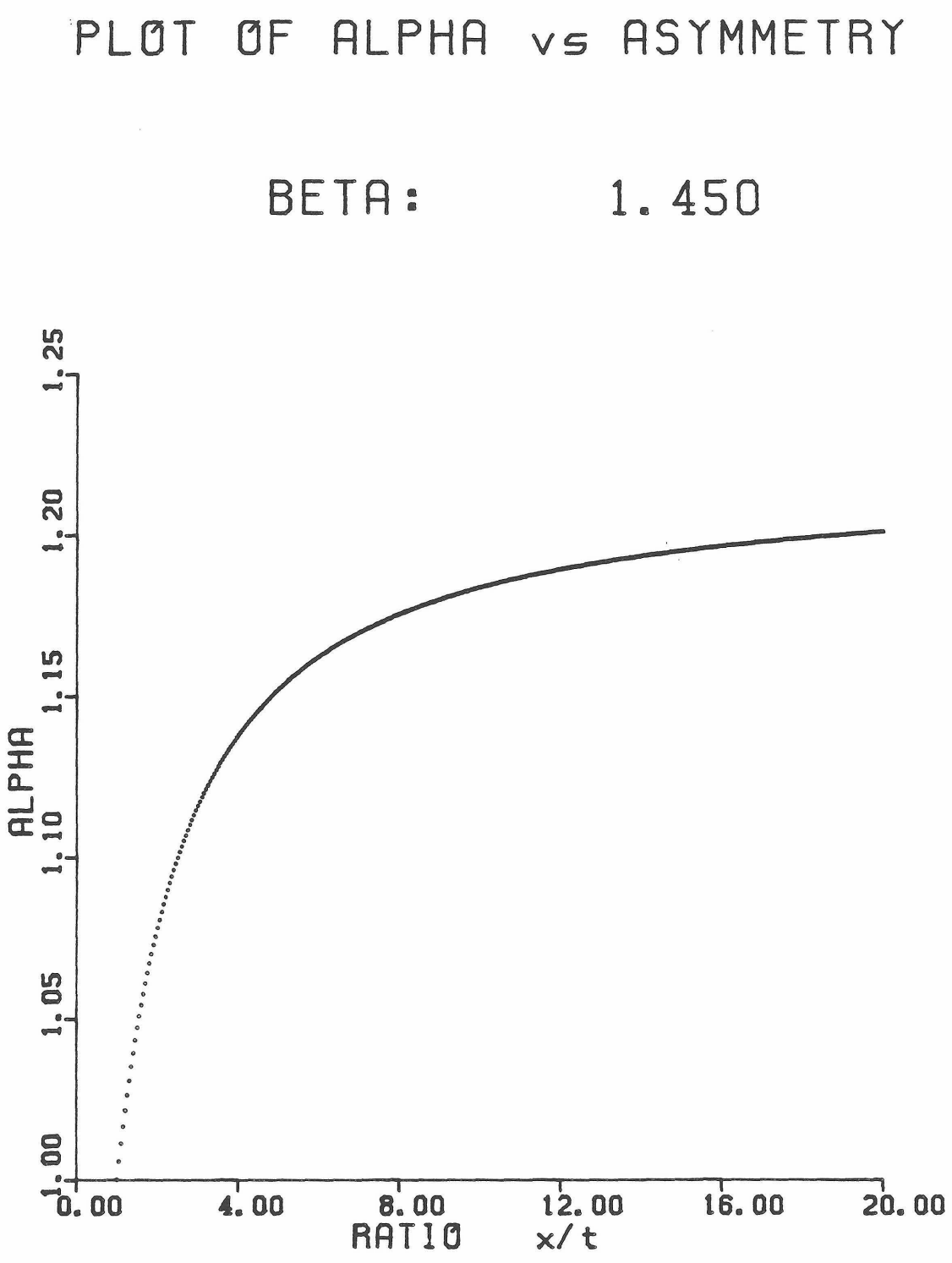
PLØT ØF ALPHA vs ASYMMETRY
BETA: 1.450
ALPHA
1.00
1.05
1.10
1.15
1.20
1.25
0.00
4.00
8.00
12.00
16.00
20.00
RATIØ x/t

Fig. 4.2